npj | materials degradation

Article

Published in partnership with CSCP and USTB

https://doi.org/10.1038/s41529-025-00720-5

Multi copper oxidase from *Micrococcus* sp. IITD107, a promising candidate for polypropylene biodegradation

Poorvika Kulshrestha[1], Richa Katiyar[2], Arif Nissar Zargar[1], Shoaib Haidar[2], Pragya Kesarwani[1], Milind Chavan[3], Balaji Bandyopadhyay[3], Debraj Chatterjee[4], Durai Sundar[1,5], Anurag S. Rathore[2] & Preeti Srivastava[1] ✉

Polypropylene (PP) is the second most abundantly used synthetic plastic which poses challenges in degradation due to its structural stability. There are limited reports on enzymatic biodegradation of PP. Here, we report degradation of commercial PP strips without any pre-treatment by a novel multi copper oxidase (MCO) from *Micrococcus* sp. IITD107. The molecular docking and simulation analysis revealed strong binding of MCO with PP. The purified enzyme and the whole cell lysate from recombinant *E. coli* expressing MCO, exhibited around 16% and 6.8% decrease (w/w), respectively in PP within 24 h at 60 °C. Changes in the functional groups and surface modification of PP were observed by FTIR, NMR and SEM. The biodegradation by-products identified were alkanes, aldehydes, ketones and a few carboxylic acids. This is the first report demonstrating the biodegradation of PP by MCO without any pre-treatment, suggesting this to have a significant role for PP degradation.

Plastics are ubiquitously in demand for their durability, cost-effectiveness, corrosion resistance, lightweight, ease of fabrication, and transparency. Global plastic production has reached around 460 million tons in 2020 and is expected to further exponentially increase to 1 billion tons by 2050[1]. At present, most plastics are highly invulnerable to natural degradation and require years for their complete degradation[2]. A recently published life cycle assessment of plastic waste has reported that about 9-15% of used plastics undergo recycling, 12% are incinerated, and 79% are disposed in landfills due to lack of required infrastructure and poor waste management plans and regulation[1,3]. As a result, >4.8 billion tons of plastic waste have been accumulated in landfills, causing significant damage to our ecosystem and eventually human health[4]. Overcoming the plastic waste accumulation is one of the major concerns of today[5].

Among all existing conventional techniques for plastic degradation, biological degradation using microorganisms such as fungi and bacteria is gaining global attention due to their possible contribution to a sustainable nature and circular plastic economy[6]. These microorganisms create a biofilm over the surface of the plastic and release hydrolyzing enzymes that depolymerize the long plastic polymer into shorter chains and/or monomers, oligo-, and di-mers, which are ultimately assimilated by microorganisms and are then intracellularly metabolized to H_2O and CO_2 or upcycled to other value-added products[7–10].

Polypropylene (PP) is the second most used petroleum-based plastic material after PE. It faces challenges in decomposing due to its high structural and thermal stability[11–13]. These properties contribute to its slow biodegradation in natural environments. Only a limited number of microorganisms, such as *Bacillus* sp., *Brevibacillus* sp., *Phanerochaete chrysoporium*, *Streptomyces ardesiacus*, and *Rhodococcus* sp., have been reported to degrade PP till date[14–16]. *Streptomyces ardesiacus* strain NBI0111 isolated from a plastic-contaminated site reduced the dry weight of PP plastic by 17.52% in laboratory conditions in a period of 90 days[17]. In another such report, *Bacillus cereus* showed 12% and *Sporosarcina globispora* showed 11% weight loss of PP film in 40 days[18]. Recently, a dioxygenase (HIS1) from rice has been identified for PP oxidation by using a culture-independent approach[19]. The enzyme required $FeSO_4$ and 2-oxoglutarate for its activity.

Laccases (EC 1.10.3.2), from the blue multi-copper oxidase (MCO) family, have been reported for their capability towards catalyzing a broad spectrum of phenolic and non-phenolic compounds[20]. These enzymes feature four copper ion binding sites[21], with copper playing a significant role in regulating their induction and activity. MCOs have not been explored for their activity towards PP. Here, we report cloning, expression, purification, and characterization of a novel MCO that has been obtained from the isolate *Micrococcus* sp. IITD107 and demonstrate its activity towards the

[1]Department of Biochemical Engineering and Biotechnology, Indian Institute of Technology Delhi, New Delhi, India. [2]Department of Chemical Engineering, Indian Institute of Technology Delhi, New Delhi, India. [3]ITC Life Sciences & Technology Centre, ITC Limited, Bengaluru, India. [4]ITC Packaging and Printing Business, ITC Limited, Chennai, Tamil Nadu, India. [5]Institute of Bioinformatics and Applied Biotechnology (IBAB), Bengaluru, India. ✉e-mail: preeti@dbeb.iitd.ac.in

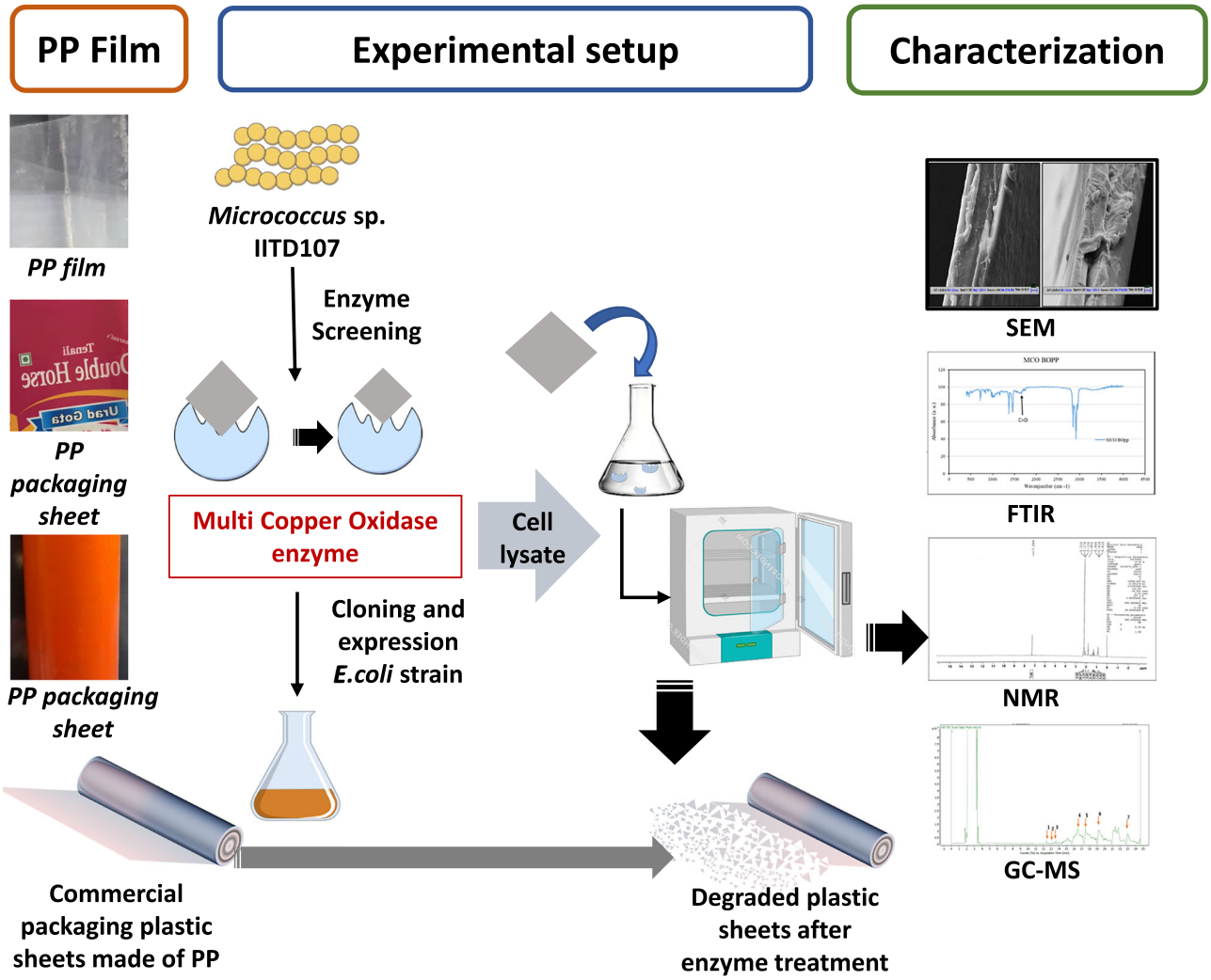

Fig. 1 | Schematic representation showing the setup for PP treatment by MCO, followed by the validation of its degradation.

degradation of PP. Commercial PP packaging strips were treated with the enzyme MCO from *Micrococcus* sp. IITD107 and biodegradation was validated by various methods (Fig. 1).

Results

Biodegradation of PP by *Micrococcus* sp. IITD107

Micrococcus sp. IITD107 has been previously reported as a member of the consortium for asphaltene biotransformation[22] and was tested to assess its ability to biodegrade PP in minimal media. Since asphaltene has a complex structure, we hypothesized that microorganisms capable of biotransforming asphaltene may degrade plastic. Interestingly, the culture grew up to an OD_{600} ~ 0.4 using PP strips as the sole carbon source at 30 °C for a period of 21 days, and approximately a 2.6% decrease in weight was observed. The maximum biomass and biomass yield coefficient obtained were 0.22 gL^{-1} and 0.2 g biomass/ mg substrate, respectively, after 21 days of growth of *Micrococcus* on PP as the sole carbon source.

Identification of a gene for multi-copper oxidase from *Micrococcus* sp. IITD107

To determine the enzyme responsible for the biodegradation of PP, the whole genome sequencing of *Micrococcus* sp. IITD107 was carried out. The genome sequence has been deposited at Genbank with Accession no. MT830855. Out of several Polycyclic aromatic hydrocarbons (PAH) degrading genes, the gene coding for MCO was selected for the following reasons: (a) MCOs were reported for their activity on polyethylene, but there were no reports on polypropylene degradation[23,24]; (b) There were no reports demonstrating gravimetric decrease in the weight of the plastic pieces by MCO as the studies reported used PE powder; (c) Furthermore, the sequence of the gene for *Micrococcal* MCO showed about 57% and 44% identity to LMCO2 (CP008950.1:146277-147827) and LMCO3(CP008950.1:195529-196575) genes reported for PE degradation from *Rhodococcus* (Fig. S2). The identities were 45% and 26% with LMCO2 and LMCO3 proteins, respectively (Fig. 2).

Multi-copper oxidase from *Micrococcus* exhibits a higher binding affinity with polypropylene

The sequence level identity suggested the MCO from *Micrococcus* to be different from the reported LMCO2 and LMCO3 from *Rhodococcus*. To further elucidate the differences, molecular docking between the enzyme and substrate was performed. The MCO extracted from *Micrococcus* sp. IITD107 is novel, and the active site of the enzyme was unknown. Blind docking was carried out with different docking parameters to allow PP to find the active site with stable interactions and the minimum binding affinity. Similarly, the LMCO2 and LMCO3 from *Rhodococcus* were selected for docking studies. A comparison of the binding affinities for different sizes of PP further revealed differences between the three enzymes. The binding affinity of 10-mer polypropylene with MCO showed the minimum binding energy, suggesting better biodegradation with MCO from *Micrococcus*sp. IITD107 as compared to that from *Rhodococcus* shown in Fig. 3A. The

% Identity Matrix		1	2	3	4
1	MCO from Bacillus	100	20.17	16.96	16.77
2	LMCO3	20.17	100.00	26.32	28.25
3	MCO	16.96	26.32	100.00	45.00
4	LMCO2	16.77	2.25	45.00	100.00

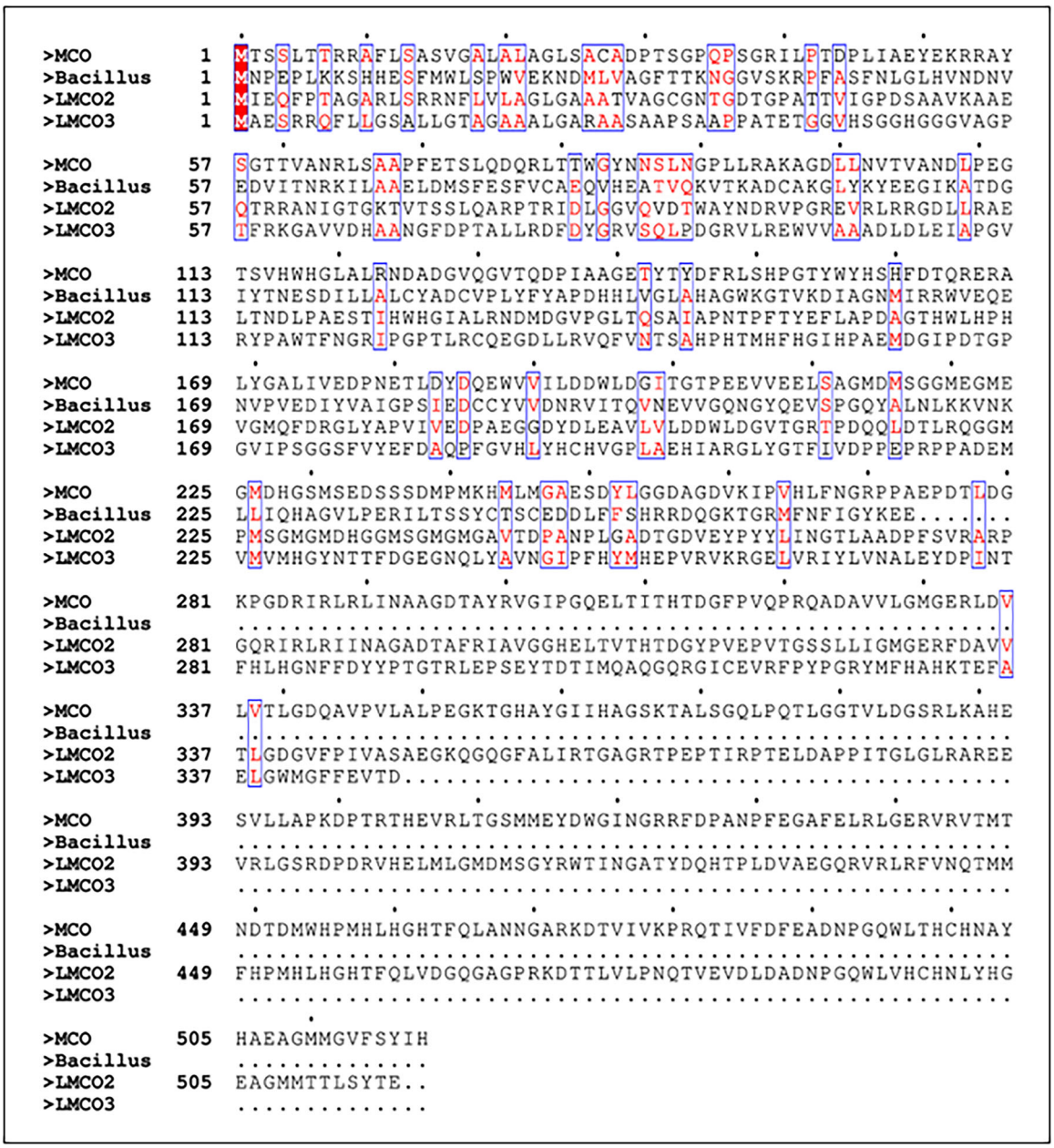

Fig. 2 | Multiple sequence alignment of the multi-copper oxidase of *Micrococcus* sp. IITD107 with that of LMCO2 and LMCO3 from *Rhodococcus opacus* and laccase from *Bacillus megaterium* at the protein level.

docking of 30-mer PP with *Micrococcus* MCO also showed stable interactions. The binding affinities from the docking studies suggested that the MCO is highly active for PP in all forms, with the highest activity observed when the size of PP was reduced to a 10-mer[25,26]. Thus, MCO from *Micrococcus* was selected for further studies.

Interaction analysis governing the stability of the complex

The 2D interactions of MCO with 10-mer PP were visualized in Discovery Studio Visualizer. The binding affinity of the substrates against the enzyme revealed that the MCO interacts with the 10-mer of PP primarily through van der Waals, π-sigma, and hydrophobic interactions with the enzyme.

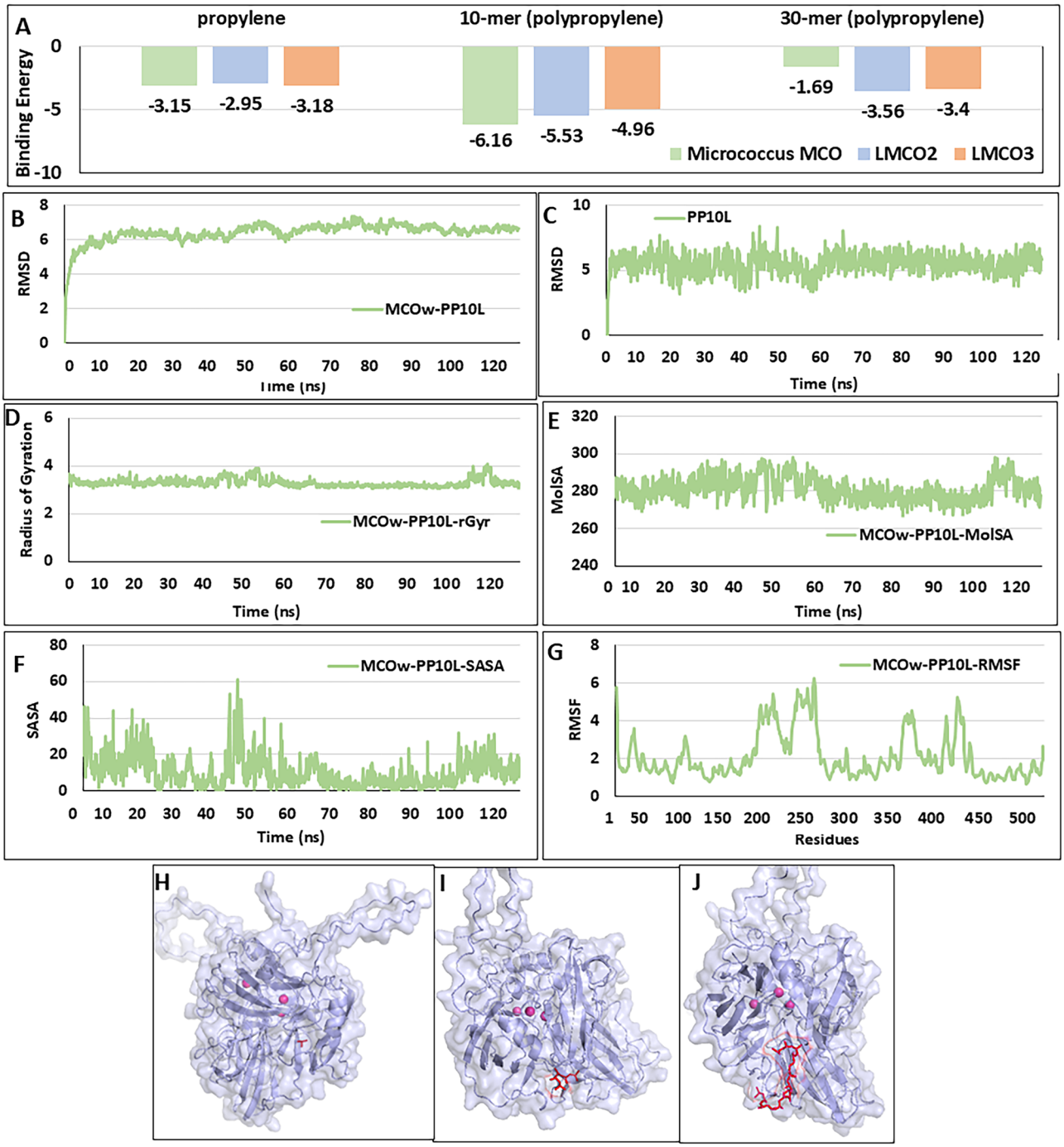

Fig. 3 | Comparison of binding affinity and stability analysis of different forms of polypropylene bound to MCO extracted from *Micrococcus* sp. IITD107. A Comparison of the binding energies of polypropylene with *Micrococcus* and *Rhodococcus* MCO. **B** RMSD plot of *Micrococcus* MCO bound to PP to assess the structural stability when bound to different plastic types. **C** Similarly, the RMSD plot of PP and PE represents their stability and conformational dynamics inside the active site of MCO. **D** Radius of gyration to measure the compactness of the complex. **E** MolSA represents the surface of PP interacting with the active site of MCO, and **F** SASA represents the surface area of the polymer exposed to solvent. **G** Root mean square fluctuation plot represents the flexibility of the amino acid during simulation in the bound state with PP. 3D representation of the binding of different sizes of PP on the surface of MCO. Protein is represented in cartoon representation with bound **H** propylene, **I** 10-mer polypropylene, and **J** 30-mer of polypropylene. Copper ions are colored as magenta, whereas substrates are colored as red in the sticks representation.

The involvement of more residues in the stable binding of PP with the MCO makes it susceptible to biodegradation. The interaction profiles of PP with MCO are presented in Fig. 4A–F.

Propylene forms a Pi-sigma interaction with an aromatic residue named HIS151 to stabilize ligands through non-covalent interactions. This interaction likely contributes to the overall stabilization of propylene within the binding site. Additionally, propylene is stabilized by hydrophobic interactions inside the active site of MCO with LEU120, ALA121, and LEU149 (Fig. 4A, B). Propylene is also supported by van der Waals interactions within the active pocket of MCO, contributing to its stability inside the active site of MCO by VAL175, TYR155, SER150, ARG148, ARG54, and LEU122. These interactions improve overall binding affinity, as validated

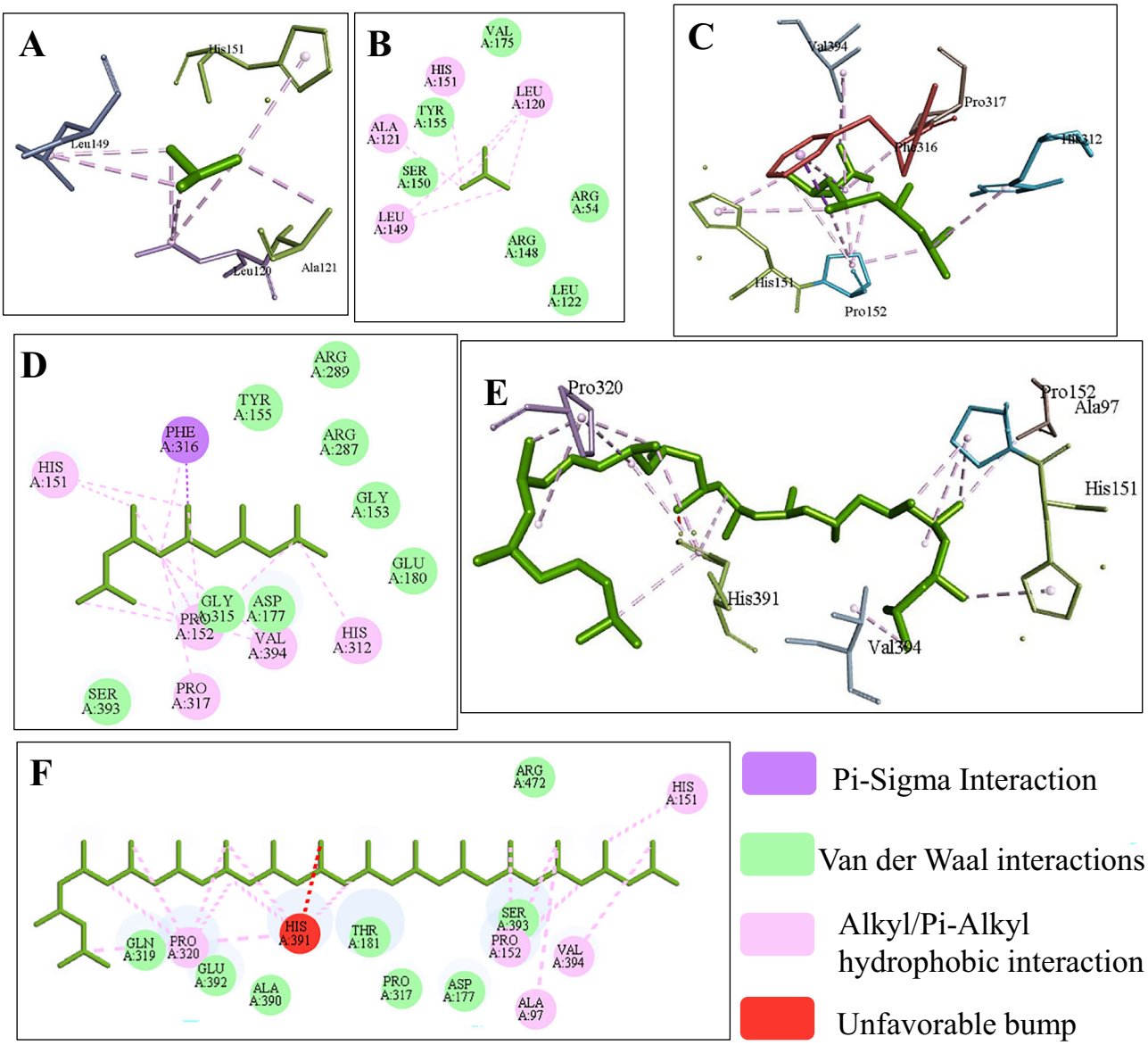

Fig. 4 | The interaction profiles of PP with MCO. A–F The interaction plot between MCO and various forms of PP. The three-dimensional representations of **A** propylene, **C** 10-mer polypropylene, **E** 30-mer polypropylene interacting with the amino acids of MCO depict the conformation and orientation, whereas the two-dimensional interaction plots of **B** propylene, **D** 10-mer polypropylene, and **F** 30-mer polypropylene with the respective amino acids in multi-copper oxidase represent the types of interactions between them. The amino acids in the three-dimensional representations are colored based on amino acid type, while the plastic polymer in the 3D representation is colored purple.

with binding energy. The combination of Pi-sigma and hydrophobic interactions allows propylene to form a more stable complex within the active site. Therefore, propylene results in having better binding affinity and catalytic activity.

The 10-mer of PP was also stabilized by a Pi-sigma interaction with PHE316 and hydrophobic interactions with HIS151, PRO152, PRO317, VAL394, and HIS312 (Fig. 4C, D). The 10-mers of PP adopted multiple conformations and searched a larger conformational space in the binding pocket compared to the monomers. Therefore, the substrates are stabilized through interactions with a broader range of residues and adopt different binding poses that also involve residues not involved in monomer stabilization. The flexibility and adaptability of the 10-mers allowed them to optimize interactions across a wider range of residues within the binding pocket. The 30-mer PP shows comparable binding energies with additional unique residues like HIS391 and PRO320 in the binding site (Fig. 4E, F). Moreover, HIS151, PRO317, and VAL394 were found to be conserved and maintain their interactions in all the variants. This analysis concludes that the longer polymer of PP variants binds predominantly to the hydrophobic surface of MCO and is stabilized by a combination of π-sigma, hydrophobic, and van der Waals interactions with minimal unfavorable contacts. It can be concluded that the 30-mer of PP exhibited similar activities to MCO. The three-dimensional structure of the protein-substrate complex reveals that both the variants of PP bind to the surface of the MCO due to its hydrophobic nature and are stabilized through hydrophobic interactions, as discussed above. The binding pose of all the variants of PP inside the active pocket of MCO is shown in Fig. 3H–J.

Stability analysis of MCO and PP complex

The structural stability and interaction mechanism of the MCO-PP complex were assessed through molecular dynamics simulations. Fig. 3B presents the variation of root-mean-square deviation for all Cα atoms in the complex over time. The average RMSD of the complex was 6.43 ± 0.49 Å.

Fig. 5 | A A table showing a list of unique enzymes expressed when *Micrococcus* was incubated with PP as the sole carbon source. **B** Graph showing transcript levels of the *mco* gene in *Micrococcus* sp. IITD107 grown with and without PP as a sole carbon source ($n = 3$).

(A)

Serial no.	Enzyme secreted with PP as carbon source	Accession No.
1	Lactonase	A0A1I7MS71
2	Amidohydrolase	A0A1I7MPY3
3	2-oxohept-3-enedioate hydratase	A0A1I7MNJ9
4	2-oxoisovalerate dehydrogenase	A0A1I7MIK1
5	Acyl-CoA hydrolase	A0A1I7MQ62
6	Zn-dependent amino-or carboxypeptidase	A0A1I7ME61
7	Putative hydrolase	A0A1I7MF03

(B)

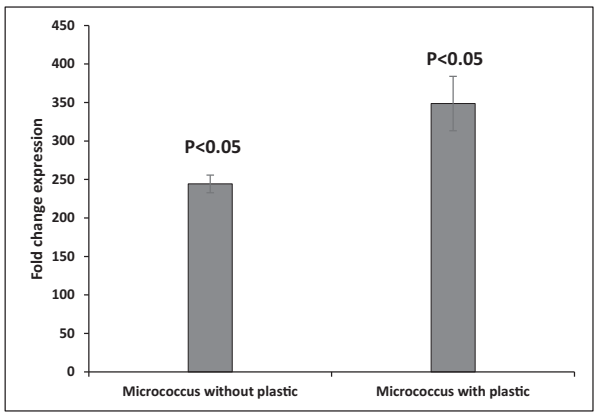

The MCO bound to PP remains stable throughout the simulation. The average RMSD of the ligand was 5.52 ± 0.79 Å, and the trend over the period of simulation represented in Fig. 3C indicates that the 10-mer propylene maintained structural stability inside the active site of MCO throughout the simulation. However, it has undergone conformational dynamics to facilitate interaction with the protein. The average radius of gyration (rGyr) of the structure was estimated as 3.29 ± 0.17 nm, indicating the relatively stable and compact structure throughout the simulation. The mean solvent-accessible surface area (SASA) of 10.67 ± 8.76 nm^2 suggested that the ligand binding did not significantly alter the overall exposure of the ligand to the solvent. The average molecular surface area (MolSA) was 281.12 ± 6.42 nm^2, further supporting the structural integrity of the complex. The root-mean-square fluctuation (RMSF) results showed an average fluctuation of 2.13 ± 1.22 Å, with higher flexibility observed in the mid region, while the rest of the protein exhibited relatively stable dynamics. The rGyr, MolSA, SASA, and RMSF plots plotted over the period of simulation are shown in Fig. 3D–G. These findings indicate that the binding of the 10-mer propylene ligand did not compromise the structural stability of the MCO complex, thereby facilitating a stable interaction. Therefore, it can be interpreted that PP forms an extensive and complex interaction with MCO. Similar findings were also observed in molecular docking studies. The change in conformation of polypropylene inside of MCO cavity during simulation was recorded and represented at an interval of 30 ns in Fig. S3A–D, respectively.

Secretome analysis of *Micrococcus* sp. IITD107 grown on PP as the sole carbon source

To identify whether the MCO is secreted in the culture supernatant of *Micrococcus* with PP as the sole carbon source, secretome analysis of the *Micrococcus* culture grown with and without PP as the sole carbon source was performed. Several different enzymes were identified in extracellular secretion, like hydratase, lactonase, amidohydrolase, oxoisovalerate dehydrogenase, copper-binding protein, etc. (Fig. 5A). Enzyme assays were performed, and MCO activity was determined in the *Micrococcus* culture by a colorimetric assay performed using 20 mM ABTS as a substrate. The colorimetric assay showed development of bluish green color and an absorbance of ~0.412 (0.14 U/ml) at 420 nm as compared to the control, which is indicative of the presence of MCO activity, thereby confirming the presence of MCO (Fig. S4).

Copper-binding protein was detected in the secretome; however, MCO was not detected in the secretome of *Micrococcus* cultures grown in the presence of polypropylene (PP). It is plausible that the enzyme is not secreted extracellularly but instead exists as a cell-bound protein. A membrane-associated MCO could facilitate direct interaction between the

bacterial cell surface and the polymer substrate, enabling localized oxidation of the PP surface and initiating its breakdown without the need for enzyme secretion into the surrounding medium. Indeed, a few well-studied examples demonstrate that bacterial MCOs can be firmly associated with the cell membrane rather than being released into the extracellular environment. For instance, the MmcO protein from *Mycobacterium tuberculosis* has been characterized as a membrane-associated MCO[27]. Similarly, in *Pseudomonas putida* GB-1, the MCO *CumA*, which catalyzes Mn(II) oxidation, is predicted to localize in the outer membrane[28]. In addition, studies on *Pedomicrobium* have shown that manganese-oxidizing MCO activity is associated with the outer cell membranes[29]. Therefore, gene expression analysis was further performed through RT-PCR to confirm the possibility of MCO being a cell membrane-bound protein.

Expression analysis of the *mco* gene in *Micrococcus* sp. IITD107

Quantitative RT-PCR analysis, performed in triplicates, showed that *Micrococcus* cultures exposed to plastic (about 5 days of incubation in PP) exhibited higher expression of the *mco* gene compared to cultures grown without plastic. The plastic-grown samples showed 348.65-fold higher expression, whereas the control cultures without plastic showed 244.24-fold change as compared to the housekeeping *gyrA* gene, representing a ~1.43-fold increase in expression (Fig. 5B). The data demonstrated a clear trend toward higher *mco* transcript levels under plastic exposure, with a p value < 0.05.

It might be possible that these copper-binding proteins act as chaperones, facilitating the uptake and transfer of copper ions from the environment to the membrane-bound MCO, as has been suggested in a few studies[30–32]. The delivery and incorporation of copper into the enzyme's active T1 Cu site could enhance the catalytic efficiency of the MCO, thereby promoting oxidative modification of the polymer chains and facilitating subsequent degradation processes. In one such study, the human copper chaperone Atox1 mediates Cu delivery to proteins that are made in the secretory pathway[33].

Biodegradation of PP by crude cell lysate of recombinant *E. coli*

The gene coding for *mco* from *Micrococcus* was cloned into an expression vector, and the expression studies were performed in *E. coli* Origami (DE3) B2 cells and *E. coli* SHuffle T7 strain. The expression was determined by analyzing crude cell lysate on an SDS-PAGE. Maximum induction in *E. coli* Origami (DE3) B2 was observed when culture was induced with 1 mM IPTG at an OD_{600} of ~0.5–0.6 and further grown for about 5 h at 37 °C (Fig. S5A). Enzyme activity of the MCO in the crude cell lysate was found to be 0.47 U/ml using guaiacol as the substrate. On the other hand, the enzyme activity of inactive mutant MCO was found to be 0.02 U/ml. The ability of the enzyme to degrade PP was assessed by incubating the whole cell lysate with commercial PP strips. About 7% decrease in the weight of PP was observed after repeated replenishment of fresh cell lysate every week for 4 weeks at 37 °C (Fig. S6). However, when the experiment was performed at 60 °C, about a 6.8% decrease in the weight of PP was observed within 24 h with respect to the initial weight by gravimetric analysis. To determine the extent of degradation, sequential transfer of the plastic strip was done after every 72 h in fresh cell lysate. An overall decrease in weight by about 24% was observed in PP after five transfers (15 days) (Fig. 6A, B). Around 2.5 mg/mL of total protein in the soluble fraction of the crude cell lysate resulted in ~6–7% degradation of a 2.5 mg polypropylene strip after incubation at 60 °C for 3 days. Further, it was observed that even after prolonged incubation for 7–14 days, the amount of degradation achieved was the same as seen in the first 3 days until unless we replenish the enzyme every 3 days. On supplementing the enzyme every 3 days, the degradation continues.

The removal rate constant (K) per day of PP samples by crude cell lysate of MCO using first-order kinetics was determined. The reduction rate constant (K) of the PP strip incubated for 15 days was calculated to be 0.018 day^{-1}. The rate constants (K) of the PP sample supported the degree of degradation activities within the PP samples.

To eliminate the possibility that the enzyme was acting on additives or impurities rather than the polymer itself, 99% pure polypropylene (PP) pellets were incubated with the crude lysate of the MCO at 60 °C for 3 days. After incubation for about 3 days, the PP pellet was found to be completely disintegrated (Fig. 6C).

Several sets of control experiments were set up to confirm the degradation activity. PP strip incubated with buffer only, crude lysate of empty pET or cell lysate of heat-inactivated enzyme did not show any change in weight.

Changes in the functional group on the surface of the PP strip

To determine any changes in the functional groups on the surface of the PP strip, FTIR and ^1H NMR were carried out. FTIR spectra showed the shift in chemical bonds and formation of carbonyl groups as compared to the control sample. FTIR analysis showed peaks at 1743 cm^{-1} and 3369 cm^{-1} in the PP (BOPP) test sample, referring to the formation of some carbonyl (C=O) and hydroxyl (O–H) groups in PP (Fig. 7A). FTIR analysis of the inactive mutant enzyme-treated PP strips was performed as a control to confirm that the observed changes were not due to any enzyme adsorption on the PP surface, but rather a result of the catalytic activity of the wild-type enzyme initiating polymer degradation. The spectra showed no similar peak at 3369 cm^{-1} or 1743 cm^{-1} corresponding to hydroxyl or carbonyl bond stretching as was seen in MCO-treated PP. A small peak at 1739 cm^{-1} was observed corresponding to carbonyl bond attack, but has a very low intensity compared to the MCO-treated sample (Fig. S7C).

The FTIR spectra of the PP strips incubated with the control samples (buffer only, empty pET, and heat-inactivated enzyme) also showed no peak of carbonyl bond attack or hydroxyl bond attachment as observed in the test sample at 1743 cm^{-1} and 3369 cm^{-1} (Fig. S7A, B, D).

In the ^1H NMR of PP, the peak at 1.829 corresponded to the CH_2 bond, which was seen to be diminishing in the test sample, and the peak at 2.154 in the test sample represented the stretching of the CH_3CO bond. (Fig. 7B).

Changes on the surface and edges of the PP strip

To observe the changes on the surface of the PP strips after enzymatic treatment, scanning electron microscopy was performed. The edges of the plastic strip appeared rough after treatment with the enzyme as compared to the control (Fig. 8). Further, cracks were observed on the surface of the treated sample (Fig. 8). The PP strip incubated with a different set of controls (Buffer, empty pET, heat-inactivated enzyme) showed smooth edges and surface (Fig. S8).

Production and purification of MCO

The cells producing MCOs were grown in the bioreactor, and the specific growth rate was estimated to be 0.25 ± 0.50 h^{-1}. Biomass productivity for the cells was calculated as 95.5 ± 2.1 mg/L/h. The expressed MCO enzyme in *E. coli* accumulated as IBs (Fig. S9A). The SDS-PAGE profile showed the molecular weight of the protein to be nearly 56.4 kDa. Total fermentation yield of MCO was calculated to be around 100 ± 1.6 mg/L of cell culture as per densitometry. IBs were estimated to be nearly 45% w/w of cell biomass with more than 87.0 ± 3.2 mg/L (w/v of culture) of MCO enzyme as per the densitometry.

Solubilized IBs exhibited better outcomes when solubilized using 4–8 M urea instead of 2 M urea concentration in the solubilization buffer (Fig. S9A). The recovery was estimated to be >92% of MCO compared to other urea concentrations (80–85% recovery). Affinity chromatography followed by on-column refolding (with the addition of $CuCl_2$) of MCO showed a purified band of MCO at a molecular weight of around 56.4 KDa (Figs. S5 and S9B, C). The densitometry analysis revealed 15.0–20.0 mg/L (w/v of culture) of purified protein. Size exclusion chromatography (SEC) analysis exhibited the purity of around 60–70% for MCO (Fig. S10A). The intact mass profile of purified MCO showed a molecular mass of 56.4 kDa, which compared well with the molecular weight obtained from the SDS-PAGE profile and estimated from the original protein sequence (Fig. S10B).

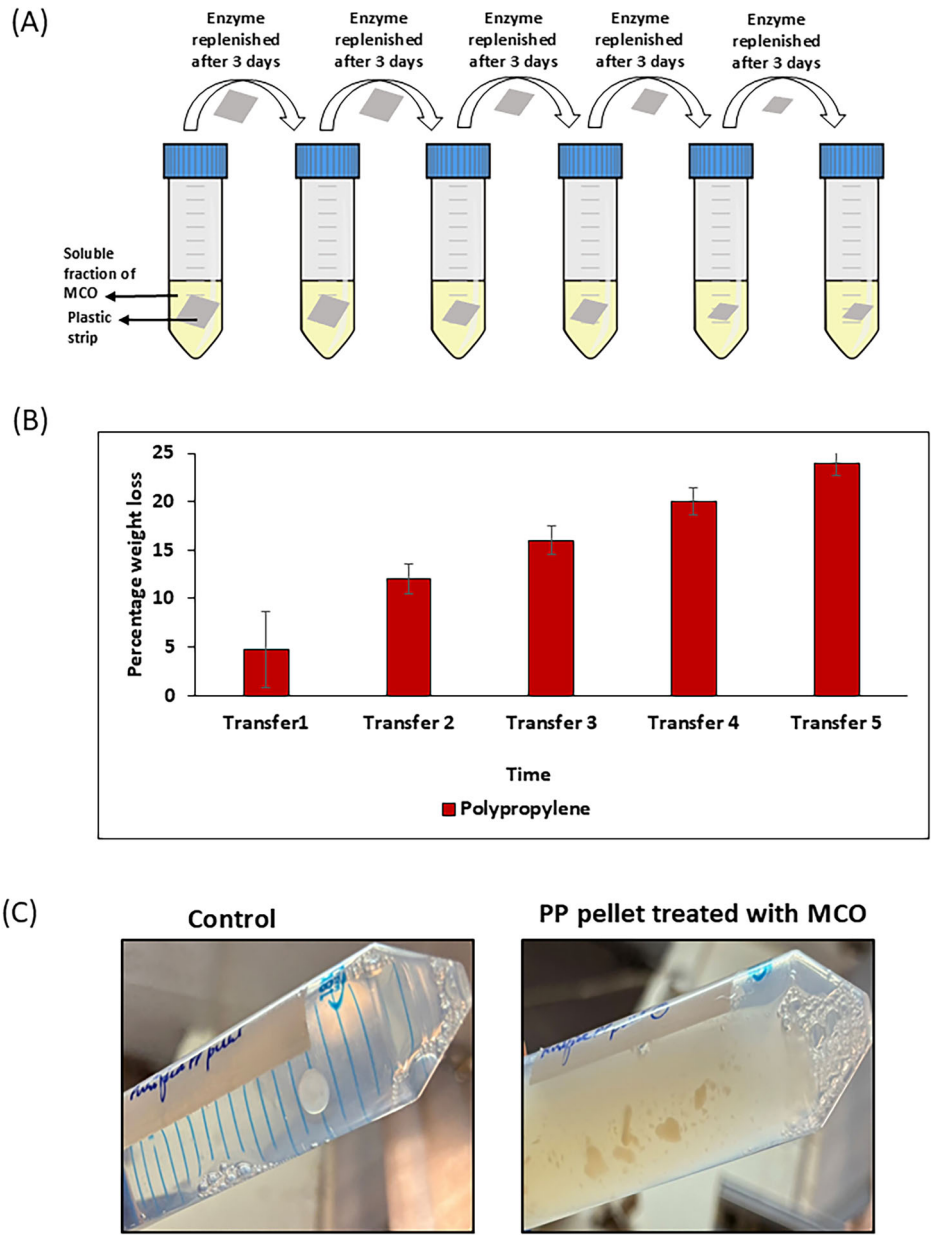

Fig. 6 | Biodegradation of PP by crude cell lysate of MCO. A Schematic representation showing PP degradation in weight with media replenishment after every 3 days, **B** Percentage weight loss of PP with whole cell lysate of MCO in about 15 days at 60 °C with repeated replenishment after every 72 h, **C** Disintegrated PP pellets (pure) after 3 days of incubation at 60 °C with crude cell lysate of MCO.

The identified peptides of MCO exhibited sequence coverage of around 80% with the original protein sequence (Fig. S5B).

Characterization of purified MCO

Enzyme activity of the MCO was found to be 0.94 U/ml using Guaiacol as substrate (4 mM). The activities in the presence of ABTS and syringaldehyde were also measured and calculated to be 0.023 U/ml and 0.020 U/ml (Fig. S11). Kinetic properties of the enzyme with all three substrates were determined by non-linear regression fitting into Michaelis-Menten kinetics. The analysis of kinetic parameters, performed in duplicates, indicated a higher K_m value of 2.230 mM, V_{max} of 8.210 mM min^{-1} for Guaiacol as compared to ABTS (K_m: 1.073 mM, V_{max}: 0.681 mM min^{-1}). Results with syringaldehyde as substrate showed less activity and ambiguous kinetic values. Optimum temperature for the improved activity of MCO was found to be in the range of 60–85 °C.

To determine the redox potential of MCO, cyclic voltammograms of the enzyme at a concentration of 1.5 mg mL^{-1} were obtained at a scan rate of 50 mV s^{-1} using a phosphate buffer solution of pH 7 as the supporting electrolyte (Fig. 9A). The anodic peaks showed potential of 0.980 V corresponding to the oxidation of MCO from its fully reduced state (Cu I) to the native state (Cu II) which is comparable to other reports published on redox potential of MCO[34,35]. In a report published in 2022, laccase isolated from *Botryosphaeria rhodina* MAMB-05 showed oxidation potential of >0.70 V vs. NHE[36].

Metabolites formed by the degradation of PP

The crude cell lysate of MCO was further evaluated for its degradation ability towards PP strips for 24 h at 60 °C. The degradation metabolites of the enzyme were then assessed using GC-MS to detect the released products. After n-hexane extraction, GC-MS analysis showed mostly alkanes like Hexane, 2,4-dimethyl, heptadecane, alcohol (Hexadecanol), aldehydes (Hexadecenal, Octadecenal) and acids (Hexadecanoic acid, Octadecanoic acid) with carbon chain lengths mainly ranging between C4 and C21 (Fig. 9B). MS analysis of degradation products of PP film showing potential degradation products is shown in Fig. S12. This initial analysis suggests a partial oxidation of the polymer chain. Alternatively, the first step is PP oxidation by MCO, ultimately leading to breaking of C–C bonds, as has been proposed already for oxygenase enzymes[19].

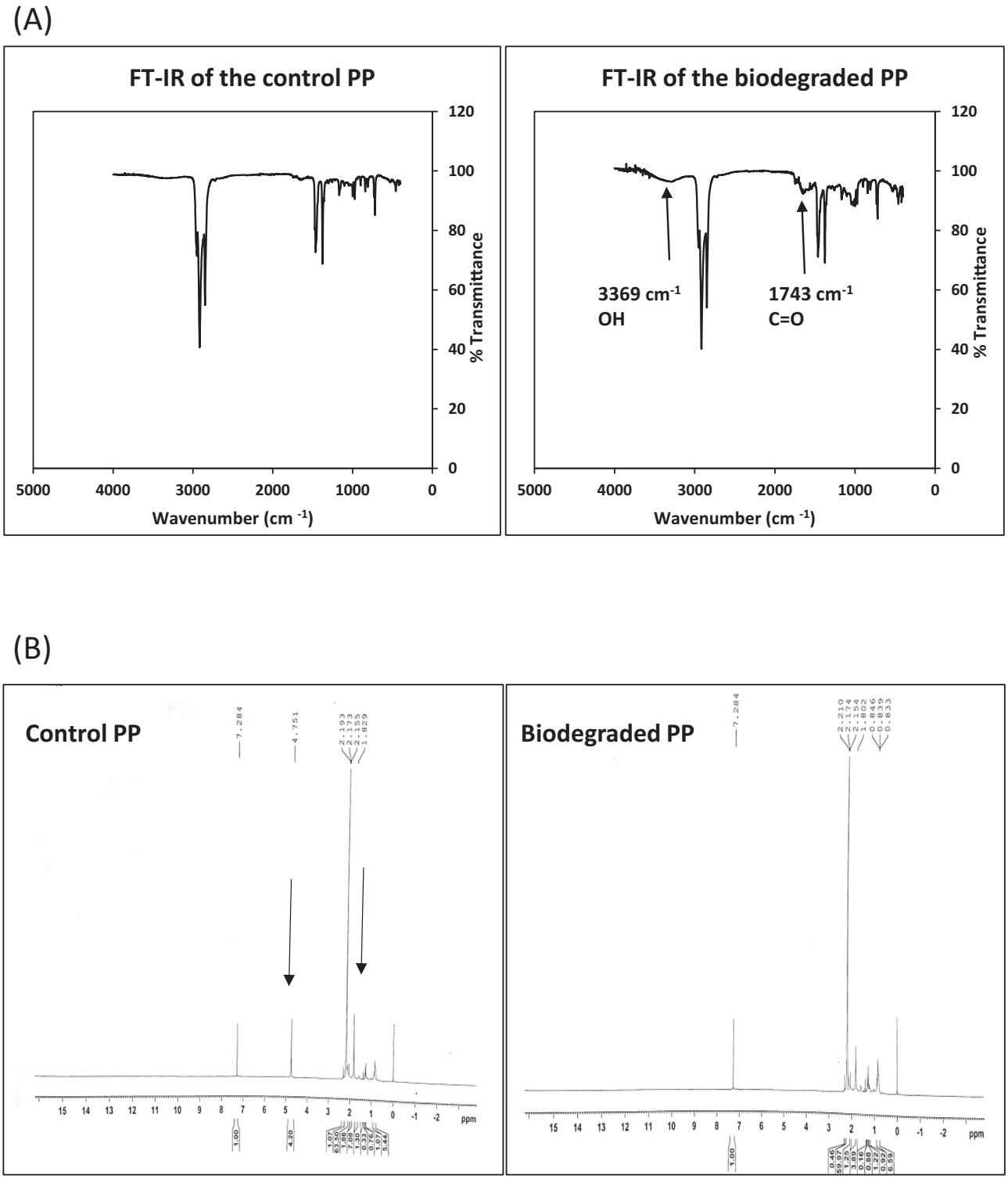

Fig. 7 | Chemical changes in the PP strip after treatment with crude lysate of MCO. A FTIR analysis of polypropylene (PP) before and after treatment with crude cell extract expressing MCO, **B** ^{1}H NMR analysis of polypropylene (PP) to identify the changes in chemical shift before and after treatment with crude cell extract expressing MCO.

MCO can catalyze the one-electron oxidation of a substrate. This initial oxidation step converts the substrate into a highly reactive free radical by one-electron oxidation. The unstable free radicals generated are highly reactive and can undergo further non-enzymatic reactions like the abstraction of hydrogen atoms from adjacent molecules, which propagates a free-radical chain reaction, coupling reactions with other radicals or molecules, or reactions with reactive oxygen species, which may be generated as intermediates in certain conditions[37]. The chain reactions and further non-enzymatic transformations can lead to their cleavage and subsequent oxidation to form carboxylic acid groups[38,39]. Baiocco et al.[40] suggested two possible mechanisms for oxidation of the substrate through laccase, which include electron transfer (ET) and hydrogen abstraction

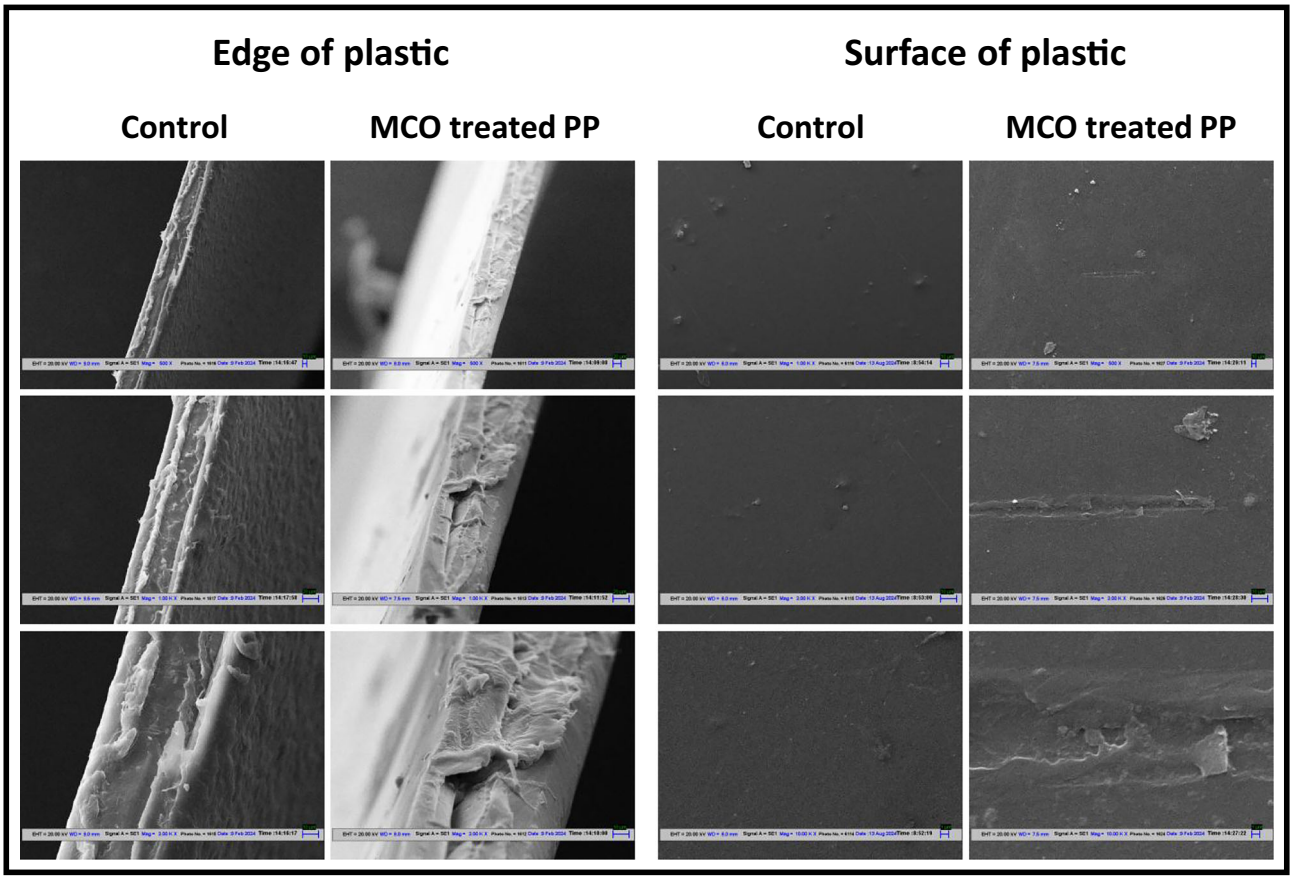

Fig. 8 | Scanning electron microscopy to determine the extent of damage of the Polypropylene (PP) after treatment with crude cell extract expressing MCO.

transfer routes[40,41]. The proposed pathway for the degradation of PP by MCO is shown in Fig. 10.

Biodegradation of commercial BOPP films by MCO

The commercial BOPP films of the size 1 × 1 cm, when treated with purified MCO resulted in a maximum of about 16% weight loss in 24 h.

Discussion

Decomposition of PP, the second most prevalent petroleum-based plastic followed by PE, offers challenges owing to its structural stability[3]. PP displays superior resistance to stress cracking, making it less biodegradable unless subjected to pre-treatment processes like prolonged exposure to high temperatures or UV radiation. PP has a methyl group replacing a hydrogen in polyethylene on every other carbon, resulting in three stereoisomers: atactic, isotactic, and syndiotactic[42]. In our study, the polypropylene that was used was BOPP, which contains isotactic PP in the central layer and ethylene propylene or ethylene butane propylene in the outer layers. It has been suggested in a study that the substitution of methyl in place of hydrogen in the β-position makes it more resistant to microbial attack[43]. This structural stability is a crucial factor contributing to its slow biodegradation in natural environments. A few studies of PP biodegradation have been described. These include bacteria like *Pseudomonas* and *Vibrio*, and the fungus *Aspergillus niger*, which have been reported to degrade PP[44]. Majorly, the studies have been carried out using pre-treated PP involving γ-irradiation[45], UV-irradiation[46–48] or thermal treatment[49] and have been shown to reduce the polymer hydrophobicity or introduce groups such as C=O or –OH, which are more susceptible to degradation. Carbonyl and hydroxyl group formation along with a decrease in viscosity have been observed during the degradation process[45,46]. *Bacillus flexus* has been shown to biodegrade UV-pre-treated PP[50]. A few studies have also reported that biodegradation of PP can be improved by using polymer blends with carbohydrates, starch or cellulose as same is used in the case of PE and polystyrene[43,44,47,49,51]. The use of these blends facilitates the adhesion of microorganisms to the surface of the polymer and acts as a co-metabolite. In this study, 2.6% degradation in weight of PP was observed without any pre-treatment of plastic by *Micrococcus* sp. IITD107. While multiple studies have reported the involvement of *Micrococcus* spp. or microbial consortia containing *Micrococcus* in the degradation of various plastics—such as polyethylene (PE), polyurethane (PU), and polyvinyl chloride (PVC)—there is a significant lack of evidence specifically implicating *Micrococcus* in PP degradation. For instance, *Micrococcus* was identified as part of a mixed microbial community that showed 4.21% and 0.25% degradation of PE bags and plastic cups, respectively, over 9 months[52]. In another report, powdered LDPE was used as sole carbon source to grow *Micrococcus luteus* IRN20 and showed 18.9% ± 0.72% weight decrease after 21 days of incubation[53]. Additionally, other studies have reported *Micrococcus*-associated degradation of PU[54] and PVC[55]. However, none of these works have directly linked *Micrococcus* spp. to PP degradation.

Therefore, our focus was to investigate the functional potential of a MCO derived from a *Micrococcus* strain towards PP. The selection of this particular MCO was also guided by bioinformatics screening and comparative analysis of oxidative enzymes, rather than solely cultivation-based approaches.

Recently, a dioxygenase (HIS1) from rice has been identified for PP oxidation by using a culture-independent approach[19]. To the best of our knowledge, this is the only enzyme reported to date for PP biodegradation. Here, we show that whole cell lysate of recombinant *E. coli* expressing the MCO isolated from *Micrococcus* sp. IITD107 resulted in a degradation of 6.8% in PP strip in 24 h and around 24% degradation in weight with repeated replenishment of crude cell lysate containing the enzyme in 15 days. Similar to the physio-chemical degradation analysis on PE film using Laccase[56], the enzyme in the present study cleaves the amorphous

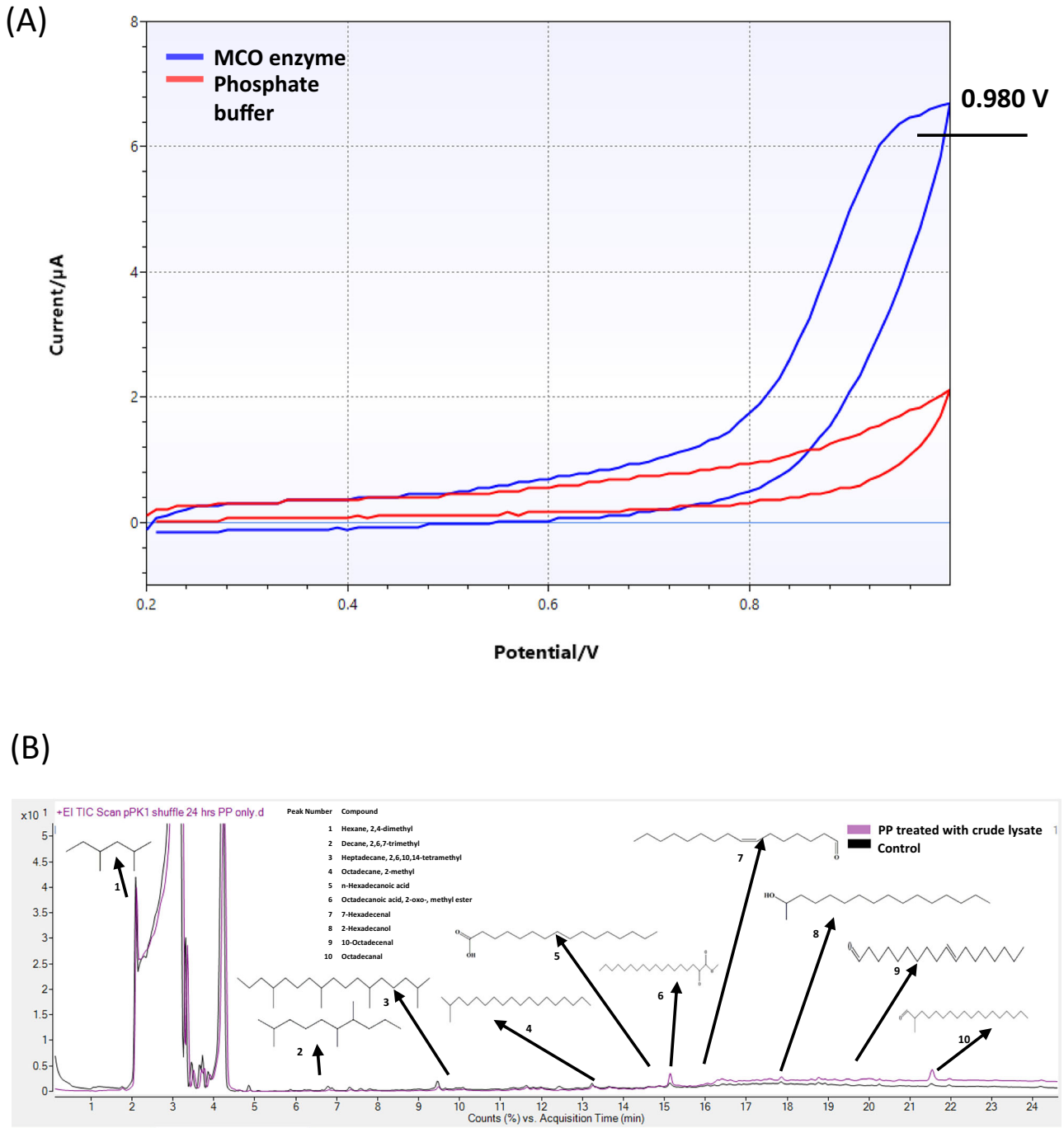

Fig. 9 | Characterization of MCO and identification of its degradation metabolites. A Protein cyclic voltammogram showing the redox potential of the enzyme as compared to the Phosphate buffer used as a control. **B** GC-MS chromatogram profiles of polypropylene oxidation by MCO enzyme. Arrows depict the major peaks detected after treatment with the enzyme, and the corresponding compound identified has been listed.

regions in PP film and forms easily accessible carbonyl groups which are further reduced into simpler forms. SEM analysis of the PP strips revealed the presence of cracks and roughness on the surface and these results were compared well with the outcomes presented by Zhang et al.[57]. The FTIR and NMR spectra of the surface revealed formation of several new functional groups such as carbonyl and hydroxyl groups. Formation of a carbonyl group is indicative of PP biodegradation, as has been reported in the literature[57–60].

The MCO was purified and showed highest activity at temperature range of ~60–85 °C and an optimum pH of 7. The optimum temperature for MCO from *Klebsiella* and *Bacillus* sp. ADR were found to be 45 °C and 40 °C, respectively[61,62]. On the other hand, laccase from *Bacillus amyloliquefaciens* and *Psychrobacter* sp. NJ228 had the temperature optima of about 80 °C and 30 °C, respectively[57,63]. In case of the MCO from *Klebsiella*, the highest activity was found to be at pH 4. The activities of laccase from *Sphingobacterium* ksn-11 and *Psychrobacter sp*. NJ228 were found to be at pH 4.5 and 3.0, respectively[57,64]. MCO from *Rhodococcus opacus* (LMCO2 and LMCO3) showed highest activities at pH 7 at 65 °C and pH 5.5 at 80 °C, respectively[23].

The K_m and V_{max} values of the purified MCO were found to be 2.23 mM and 8.21 mM min^{-1}, respectively, for Guaiacol. These values compare well with the values obtained from LMCO2 and LMCO3 along with other MCO mentioned in the literature. The K_m and V_{max} values were 1.63 mM and 0.06 mM min^{-1} for LMCO2 and, 0.28 mM and

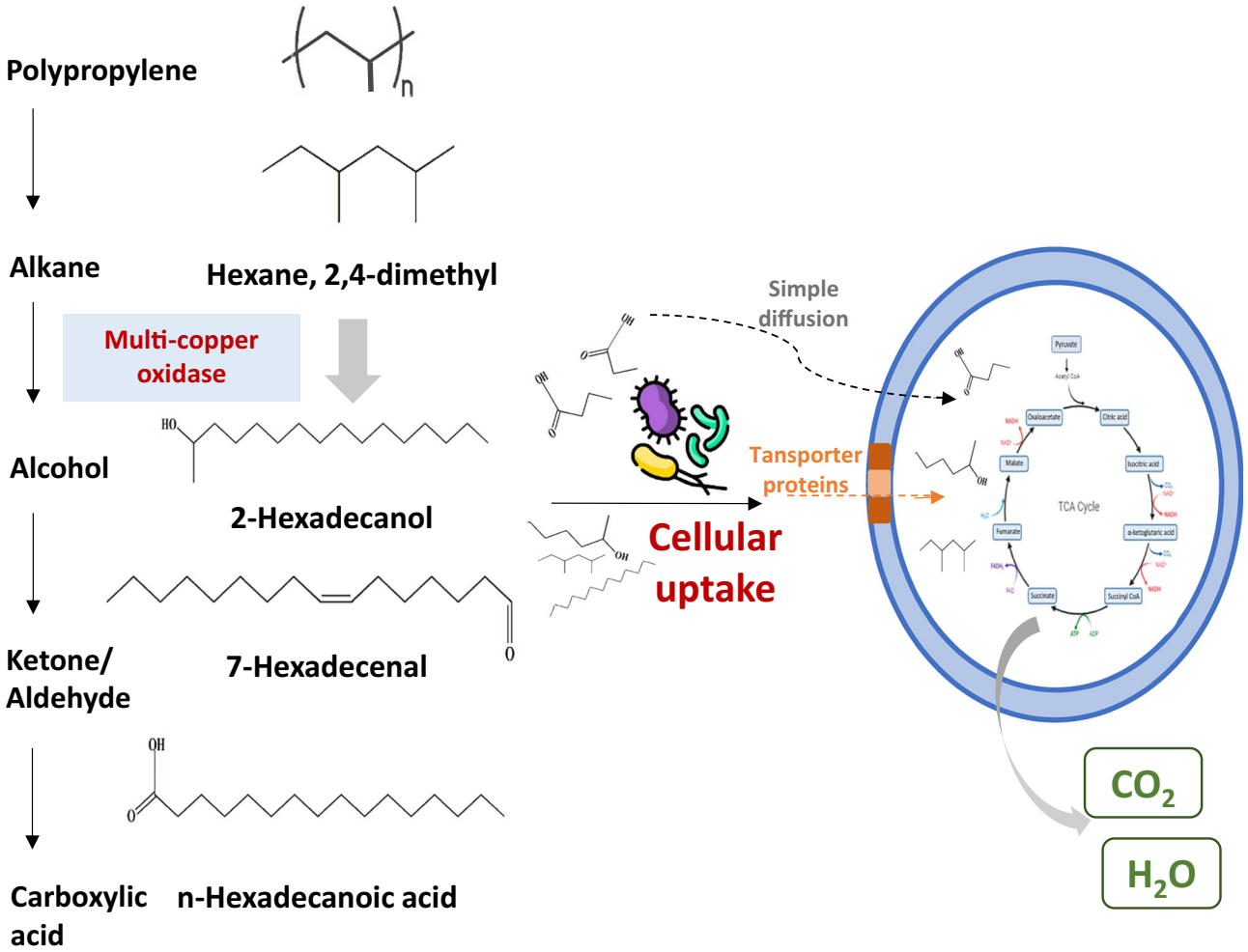

Fig. 10 | Proposed pathway for biodegradation of polypropylene.

0.02 mM min^{-1} for LMCO3, respectively, when ABTS was used as a substrate[23]. The K_m and K_{cat} of a bacterial laccase (a type of MCO) isolated from Antarctic Sea ice psychrophile *Psychrobacter* sp. NJ228 were reported to be 1.44 mM and 42.65 s^{-1}[57]. The kinetic parameters of purified laccase from *Sphingobacterium* ksn-11 were calculated to be 2 mM K_m and V_{max} of 33 U mg^{-1} using ABTS as substrate[64]. The kinetic parameters of rLAC from *Bacillus amyloliquefaciens* were evaluated at its optimum temperature and pH using ABTS as the substrate based on the Michaelis-Menten equation by non-linear regression. The K_m and V_{max} values of rLAC were 1.9 mM and 4.99 µmol/min/mg, respectively[63].

The binding affinity with PP was studied. Recently binding energies were analyzed in silico for various enzymes with different plastics[65]. The plastics were polyamide, polycarbonate, polyethylene terephthalate, polyvinyl chloride, polymethyl methacrylate and polyurethane. No studies were carried out on PP with MCO. Also, the ligand selected was monomer in their studies. To simulate natural conditions, we selected monomer, 10-mer and 30-mer PP for docking. Interestingly, higher binding affinities were observed with 10-mer as compared to monomer or 30-mer.

A comparative structural analysis was performed between the predicted 3D structure of *Micrococcus* MCO and the crystal structure of a well-characterized bacterial MCO (PDB ID: 3V9E). The alignment yielded a root-mean-square deviation of 1.428 Å, indicating substantial structural similarity, especially within the catalytic domain (Fig. S13A). The copper-binding residues in the *Micrococcus* MCO were H118, H501, and H158 (putative T1 site); H460 and H499 (T2 site); and H455, C500, and H505 (T3 site). The three-dimensional representation of residues stabilizing copper ions inside the *Micrococcus* MCO is shown in Fig. S13B–D. These residues are positioned in a spatial arrangement comparable to the corresponding metal-coordinating residues in 3V9E. This conservation of three-dimensional geometry is considered functionally more significant than primary sequence similarity as ET and catalytic activity in MCOs depend on precise spatial arrangement of copper ligands. This spatial conservation of metal-binding residues like histidine and cysteine in defined geometric configurations strongly suggests the preservation of the characteristic trinuclear copper cluster found in canonical MCOs. Hydrophobic surface mapping further revealed a non-polar patch near the active site region, potentially facilitating interactions with hydrophobic polymeric substrates like polypropylene.

The molecular docking of the *Micrococcus* MCO with polypropylene revealed a distinct set of amino acid residues interacting with PP through Pi-sigma interaction (PHE316) and hydrophobic interactions (HIS151, PRO152, PRO317, VAL394, and HIS312). The *Micrococcus* MCO interacts with polypropylene through hydrophobic interaction indicating a potentially broader and more flexible substrate-binding site.

The purified enzyme resulted in a maximum of about 16% degradation of PP in 24 h. About 12.27% degradation of PP was reported by HIS1 enzyme in 15 days[19]. Enzyme-driven breakdown of polymers, known as biocatalytic depolymerization, is now seen as an effective and eco-friendly method for treating and recycling plastics[66]. To the best of our knowledge, the present study reports the highest and fastest biodegradation activity of the MCO to date. Protein engineering for MCO could be employed to improve the efficiency of biodegradation in the future. Random mutations can be introduced into the gene using methods like error-prone PCR, DNA shuffling, or using enzymes like mutazyme to generate a library of variants

and screening through them for improved activity. Mutations in or around the active site can be done through site-directed mutagenesis by inverse PCR or using mutagenic primers to improve the affinity for substrate binding, improve thermostability, or enhance the activity at ambient temperatures. Machine learning or computational studies can be done to engineer the flexible loops around the T1 copper sites to enhance the substrate accessibility and thereby improve the catalytic efficiency of the enzyme. A directed evolution study for the hyperthermostable MCO from *Pyrobaculum aerophilum* (McoP) identified a single F290I mutation that increased specific activity by approximately 12-fold, by increasing the flexibility of a loop near the T1 copper center and improving ET between enzyme and substrate, thereby improving catalytic activity[67]. In a similar study published in 2021, mutations (M470L and M470F) were introduced into the axial ligand of the T1 copper atom of an MCO, successfully shifting its redox potential positively and increasing its catalytic activity for applications in biofuel cells[68].

This is the first report demonstrating the degradation of commercial PP strips by MCO without any pre-treatment. The MCO was isolated from a strain which was reported for asphaltene biotransformation. The study opens a new possibility of exploring a large reservoir of PAH/TPH (Total Petroleum Hydrocarbon) degrading strains and their enzymes for plastic biodegradation. The MCO identified was novel by sequence alignment. Further molecular docking and simulation studies were carried out using different forms of PP (monomer, 10 mer and 30 mer) which has not been reported in the past. The purified MCO exhibited up to 16% polypropylene (PP) degradation in weight as compared to control. The repeated replenishment of the whole cell lysate of *E. coli* expressing MCO resulted in about 24% PP degradation in weight in a span of 15 days. Our results suggest MCO from *Micrococcus* sp. IITD107 to be a promising candidate for PP degradation.

For a broader and long-term application, scale-up in bioreactors can be performed and further applied in the real environmental conditions in the treatment of plastic waste, where the enzyme can be employed in immobilized or lyophilized forms and deployed at landfill sites or wastewater treatment facilities, where it may act directly on plastic waste under ambient environmental conditions. Immobilization of the enzyme on suitable supports can enhance its operational stability, catalytic efficiency, and resistance to environmental fluctuations, thereby extending its functional lifespan, but comes with certain mass transfer limitations for commercial scale applications[69,70]. Alternatively, lyophilized enzyme formulations can be easily stored, transported, and dispersed at disposal sites, offering a convenient approach for large-scale applications.

Methods

Materials

The plastic sheets for PP (biaxially oriented polypropylene (BOPP)) was obtained from ITC Limited, India. Commercially used BOPP films used in packaging of food, confectionaries and tobacco were used in the study. All media components, buffers and their components, inducer, protease inhibitor, etc. used were of analytical grade and procured from HiMedia, India and Sigma-Aldrich, USA.

Bacterial strains and plasmid

Escherichia coli DH5α (for cloning), *Escherichia coli* Origami (DE3) B2 and *Escherichia coli* SHuffle T7 (for expression) were used in this study. *Micrococcus* sp. IITD107 has previously been reported to be a member of a consortium involved in the biotransformation of asphaltene[22]. This was tested for its ability to biodegrade PP in minimal media. The minimal media contained (per L): 2 g Na_2HPO_4, 1 g KH_2PO_4, 3.59 g NH_4Cl, 0.4 g $MgCl_2$, 17 mg $(NH_4)_2SO_4$ and was supplemented with filter-sterilized trace elements (1 mg/ml). The composition of the trace elements was (per L): 0.05 g KI, 0.05 g LiCl, 0.80 g $MnCl_2.4H_2O$, 0.50 g H_3BO_3, 0.10 g $ZnCl_2$, 0.10 g $CoCl_2.6H_2O$, 0.10 g $NiCl_2.6H_2O$, 0.05 g $BaCl_2$, 0.05 g $(NH_4)_6Mo_7O_{24}.2H_2O$, 0.50 g $SnCl_2.2H_2O$ and 0.10 g $Al(OH)_3$. The strain was incubated with 10 mg of PP as sole carbon source in minimal medium at 30 °C for a period of 21 days and gravimetric determination was performed to assess the biodegradation activity.

For protein expression studies, cells were cultured in Luria-Bertani (LB) medium supplemented with 50 µg/ml kanamycin, grown at different temperatures and 180 rpm. In case of *E. coli* Origami (DE3) B2, cells were induced with 1 mM IPTG (Isopropyl β-D-1-thiogalactopyranoside) at an OD_{600} ~0.5–0.6 and further cultivated at 37 °C for 5 h at 180 rpm. In the case of the *E. coli* SHuffle strain, the induction was performed with 0.5 mM IPTG, and the cultivation temperature was 30 °C. Post-induction, cells were incubated at 18 °C overnight.

Secretome analysis of *Micrococcus* sp. IITD107

The *Micrococcus* culture grown for 21 days up to an OD_{600} of 0.38 with polypropylene (PP) as the sole carbon source was centrifuged at 5000 rpm for 10 min. For control experiment, the culture was grown to an OD_{600} of 3.35 in the presence of Sucrose (17 g/L) as carbon source instead of PP strip. The supernatant was carefully collected, and the centrifugation step was repeated three times to ensure complete removal of cells. The resulting cell-free supernatant was then lyophilized and subjected to secretome analysis. For sample preparation, 25 µg protein sample was first reduced with 5 mM Tris (2-carboxyethyl) phosphine (TCEP) and subsequently alkylated with 50 mM iodoacetamide. The protein was then digested with Trypsin at a 1:50 Trypsin-to-lysate ratio for 16 h at 37 °C. After digestion, the mixture was purified using a C18 silica cartridge and then concentrated by drying in a speed vac. The resulting dried pellet was resuspended in buffer A, which consists of 2% acetonitrile and 0.1% formic acid.

Mass spectrometric analysis of peptide mixtures

For mass spectrometric analysis, all the experiments were performed on an Easy-nLC-1000 system (Thermo Fisher Scientific) coupled with an Orbitrap Exploris 240 mass spectrometer (Thermo Fisher Scientific) and equipped with a nano electrospray ion source. 1 µg of peptide sample was dissolved in buffer A containing 2% acetonitrile/0.1% formic acid and resolved using a Picofrit column (1.8-micron resin, 15 cm length). Gradient elution was performed with a 0–38% gradient of buffer B (80% acetonitrile, 0.1% formic acid) at a flow rate of 500 nl/min for 96 min, followed by 90% of buffer B for 11 min and finally column equilibration for 3 min. Orbitrap Exploris 240 was used to acquire MS spectra under the following conditions: Max IT = 60 ms, AGC target = 300%; RF Lens = 70%; R = 60 K, mass range = 375 − 1500. MS2 data was collected using the following conditions: Max IT = 60 ms, R = 15 K, AGC target 100%. MS/MS data was acquired using a data-dependent top20 method dynamically choosing the most abundant precursor ions from the survey scan, wherein dynamic exclusion was employed for 30 s.

Samples were processed, and the RAW files generated were analyzed with Proteome Discoverer (v2.5) against the Uniprot reference database. For dual Sequest and Amanda search, the precursor and fragment mass tolerances were set at 10 ppm and 0.02 Da, respectively. The protease used to generate peptides, i.e., enzyme specificity, was set for trypsin/P (cleavage at the C terminus of "K/R": unless followed by "P"). Carbamidomethyl on cysteine as fixed modification and oxidation of methionine and N-terminal acetylation were considered as variable modifications for database search. Both peptide spectrum match and protein false discovery rate were set to 0.01 FDR.

Quantitative RT-PCR for gene expression analysis of mco in *Micrococcus* sp. IITD107

The quantitative RT-PCR study was performed to determine the differential expression, if any, in *mco* grown in minimal media with PP or sucrose as the sole carbon source. Total mRNA was isolated using GSure Bacterial RNA Isolation Kit (GCC, India) as per the manufacturer's protocol. The concentration of RNA was measured using nanodrop. Then, 1 µg of isolated RNA was used for complementary DNA (cDNA) synthesis using Verso cDNA Synthesis Kit (Thermo Fisher Scientific, USA) and qRT-PCR was performed. For setting up the quantitative RT-PCR experiment DyNAmo color flash SYBR Green RT-qPCR master mix of Thermofisher was used. The housekeeping gene *gyrA* was taken as the control for expression analysis

to analyze the fold change of the *mco* gene. All values were measured in triplicates and error bars were calculated through standard deviation of the same.

Isolation of genomic DNA from *Micrococcus*

The isolation of genomic DNA was done as per the procedure described by Singhi et al.[71].

Cloning of multi-copper oxidase gene in pET29a

The *mco* gene was amplified from the genomic DNA of *Micrococcus* sp. IITD107 using primers PK_Multi Copper Oxidase_FP (5′ GTACCATATGATGACCTCCTCACTGACCACCC 3′) and PK_Multi Copper Oxidase_RP (5′ AGTCAAGCTTGTGGATGTACGAGAAGACGCCCA 3′). Amplified *mco* was gel purified and digested with NdeI and HindIII enzymes and ligated into pET-29a + vector digested with same restriction enzymes. The ligation mixture was transformed in *E. coli* DH5α cells and the positive colonies were screened by colony PCR. The plasmid constructed was further confirmed by restriction digestion and sequencing and named as pPK1.

Site-directed mutagenesis to generate the inactive mutant of MCO

Site-directed mutagenesis was performed to construct a catalytically inactive mutant by mutating the cysteine residue at the T1 copper site (500th position) to an Alanine residue, i.e., C500A (TGC converted to GCG). The insert was prepared by amplifying the entire pPK1 plasmid through Inverse PCR with a pair of mutant primers SDM_Inactive_FP (5′GTGGC TGACCCACGCGCACAACGCCTACC 3′) and SDM_Inactive_RP (5′ GGTAGGCGTTGTGCGCGTGGGTCAGCCAC 3′). The amplified product was eluted and then allowed to self-ligate using T4 DNA ligase. The ligation mixture was transformed into the DH5α strain of *E. coli*, and positive colonies were screened through colony PCR by using PK_Multi Copper Oxidase_FP and PK_Multi Copper Oxidase_RP primer pairs (Fig. S1A). The constructed plasmid, named pPK2, was transformed into *E. coli* SHuffle T7 strain and expression studies and degradation experiments were performed.

Expression studies

The constructed plasmid pPK1 was used to transform *E. coli* Origami (DE3) B2 and *E. coli* SHuffle T7 strain. The culture was induced by adding 1 mM IPTG at an OD_{600} ~ 0.4–0.6 and further incubated at 37 °C with sampling at 3 h, 5 h, and overnight for expression analysis. For expression in the SHuffle strain, the cells were grown at 30 °C, induced at OD_{600} ~ 0.4–0.6 with 0.5 mM IPTG, and grown at 18 °C overnight. The cells were then harvested by centrifugation at 5000 rpm for 10 min at 4 °C. The supernatant was discarded, and pellets were stored at 4 °C. The pelleted cells were resuspended in 5–10 ml of Lysis buffer (50 mM Tris-Cl (pH 7), 300 mM NaCl, 0.5% Tween-80, 1% Glycerol, and 1 mM PMSF) and were sonicated at 35% amplitude for 20 min (8 s pulse on and 17 s off) in the sonicator (Sonic & Materials Inc., USA). The sonicated cell lysate was then centrifuged at 8000 rpm for 10 min at 4 °C. The pellet and the supernatant were separated in different tubes and stored at −20 °C until further analysis. The total cellular protein was analyzed on a 12% SDS-PAGE. The constructed plasmid pPK2 containing the C500A mutation in the MCO was transformed into *E. coli* SHuffle T7 strain and expression studies were performed in a similar manner as described above (Fig. S1B).

Production of MCO

A single colony of *E. coli* Origami (DE3) B2 harboring the plasmid pPK1 was used to inoculate two different 500 ml Erlenmeyer flasks containing 250 ml of LB-Miller medium and incubated at 37 °C, 180 rpm for overnight. This was used as the seed culture for production of MCO in a 15 L bioreactor (Applikon, USA). The dissolved oxygen (DO) concentration was maintained at 30% of saturation, first by changing the agitation speed between 200 and 500 rpm, after that, the supplied air was enriched with pure oxygen up to 20%. The airflow rate during the batch phase was supplied at the rate of 0.75 vvm to 1 vvm. The pH was controlled at 7.35 ± 1.2 by adding ammonia (3 N) and phosphoric acid (2 N). The temperature for the cultivation was maintained at 37 °C for entire batch operation. The filter-sterilized kanamycin (50 µg/ml) was added to the media, and inoculation with 5% of the seed culture was performed using a peristaltic pump (Masterflex). The optical density (OD) of cells was checked every 1 h at 600 nm. Once the cells' reached the mid-log phase, the induction was performed using 1 mM IPTG and protein expression was allowed for the next 5 h. The culture was harvested by centrifugation at 7000 rpm for 10 min at 10 °C. The cell pellets were washed using phosphate buffer saline; PBS (NaCl-0.137 M, KCl-0.0027 M, Na_2HPO_4-0.01 M, KH_2PO_4-0.0018 M) of pH 7.4. The pellets (1 gram) were placed in the ice and resuspended in the 10 ml lysis buffer (50 mM Tris-Cl + 50 mM NaCl + 0.5 mM EDTA + 1 mM PMSF) of pH 8. The sonicator (Oscar Ultrasonics, India) with 70% amplitude, and 30 s on and 15 s off cycle for 20 min was used to lyse the cells. Lysed cells were centrifuged at 10,000 rpm for 20 min at 4 °C to obtain inclusion bodies (IBs). The supernatant was then discarded, and pellets/IBs were stored at −20 °C for further analysis.

Solubilization and purification of MCO

Solubilization of IBs was carried out using a solubilization buffer (pH 8.5) i.e., 100 mM NaCl and at different concentrations of urea (2–8 M). The IBs with the solubilization buffer were kept for stirring at room temperature for 1 h, followed by adding 1 mM DTT and kept for an additional half an hour to obtained solubilized inclusion bodies (SIBs).

The solubilized MCO enzyme solution was loaded onto a HisTrap HP column (Cytiva, bed volume, 5 ml) for purification using affinity chromatography, followed by refolding of the MCO in the AKTA purification system (AKTA 150 Pure, Cytiva). In a typical run, 5 ml of SIBs were injected to the column, regenerated and washed with 10 column volume (CV) of binding buffer containing 20 mM Tris-HCl (pH 8.0), 500 mM NaCl, 6 M guanidine HCl, 5 mM imidazole and 1 mM 2-mercaptoethanol followed by 10 CV of washing buffer containing 20 mM Tris-HCl (pH 8.0), 500 mM NaCl, 6 M urea, 20 mM imidazole and 1 mM 2-mercaptoethanol.

On-column refolding for MCO was performed by replacing the wash buffer to a refolding buffer (20 mM Tris-HCl (pH 8.0), 500 mM NaCl and 20 mM imidazole) using a linear gradient over 30 CV. Refolding was performed with the addition of $CuCl_2$ (1 mM) to the refolding buffer. After washing with 5 CV of refolding buffer, the MCO was eluted with 10 CV of elution buffer (20 mM Tris-HCl pH 8.0, 500 mM NaCl and 500 mM imidazole).

The fractions with refolded MCO were pooled and concentrated to 5 ml using an Amicon Ultra-15 Centrifugal Filter Unit (60 kDa MWCO). The purified and concentrated samples were checked for its purity using standard SEC in a Superdex 200 column (Thermo Scientific). The peaks were resolved and eluted with the buffer (20 mM Tris-HCl pH 8.0, 150 mM NaCl, 1 mM $CuCl_2$). The purified sample was analyzed on a 12% SDS-PAGE.

Enzymatic assay

Enzymatic assay was performed with purified enzyme using guaiacol (ε: 6.740 mM^{-1} cm^{-1}) as the substrate in 100 mM Sodium Acetate buffer, pH 5. The change in the absorbance of the reaction mixture with guaiacol was monitored for 5 min of incubation by measuring the absorbance at 470 nm in a UV Spectrophotometer. One unit of enzyme activity was defined as the amount of enzyme that oxidized 1 µmol of guaiacol in 1 min[72].

$$\text{Enzyme activity}(\text{U/ml}) = \frac{\frac{A470}{min} \times 4 \times Vt}{\varepsilon \times \text{Vs}}$$

Where, Vt is the final volume of reaction mixture (ml), Vs is the sample volume (ml), ε is the extinction coefficient of guaiacol (6.740/mM/cm), (4 has been derived from unit definition and principle)[72].

The optimal temperature (T_{opt}) was determined on guaiacol (final concentration of 4 mM) in the range 25–95 °C in Sodium acetate buffer (pH 5).

Substrate specificity was determined at optimal catalysis conditions with Guaiacol, 2,2'-azino-bis (3-ethylbenzothiazoline-6-sulfonic acid) (ABTS, 420 nm, ε: 36 $mM^{-1}cm^{-1}$) and Syringaldehyde (370 nm, ε: 14.7 $mM^{-1}cm^{-1}$) at different concentrations from 0.4 to 5 mM by monitoring the change in absorbance for 5 min. The experiment was performed in duplicates.

Determination of enzyme kinetics parameters

Kinetic parameters of the enzyme were examined at different concentrations of guaiacol, ABTS, and syringaldehyde (0.4–5 mM) in Sodium Acetate buffer (100 mM, pH 5) in duplicates and calculated with Graphpad Prism 8 software by fitting into a non-linear regression model using the Michaelis-Menten equation[57,73] by monitoring the change in absorbance for 5 min. All values were measured in duplicates, and error bars were calculated through the standard deviation of the same.

Determination of the redox potential of the enzyme

The redox potential of the enzyme was determined through protein cyclic voltammetry. CV measurements were performed on a MultiPalmSens4 Multi-channel Potentiostat connected to a Screen Printed Electrode chip obtained from Metrohm. It comprised a carbon working electrode, a reference electrode of Silver, and a Platinum as the auxiliary electrode, and 6 µl of purified protein (1.5 mg/ml) sample was loaded on it. Initially, the scanning potential from 1.0 to −0.5 V (50 mV s^{-1}) was selected to convert the native enzyme into the fully reduced state. Afterwards, the electrode potential was varied from 0.2 to 1.0 V in cyclic phases, and the oxidation potential of the laccase (1.5 mg mL^{-1}, phosphate buffer) was registered[36].

Degradative activity of MCO on polypropylene

Activity of MCO was evaluated using powdered, pellet, and strip forms of PP as substrates in duplicates. Reaction containing cell lysate of MCO was incubated with 2 mg/1 × 1 cm of PP strip at 60 °C, 120 rpm in 10 mM phosphate buffer. The PP strip incubated without the enzyme was used as a control. The degradation activity was then monitored at 24 h and evaluated by GC-MS.

The degradation activity of the enzyme using the PP strip was also examined with the whole cell lysate and purified MCO, keeping a 1:1 ratio of enzyme with the substrate. The $CuCl_2$ (400 µM) was added before putting it at 60 °C, 120 rpm for incubation in case of the whole cell lysate. The crude cell lysate and purified enzyme were incubated for 24 h, and then gravimetric analysis was performed. The gravimetric weight was determined using an analytical balance with a sensitivity of 0.0001 g (Sartorius BSA224S-CW) and an accuracy of 0.1 mg. The PP samples were removed after the degradation experiment, washed with 70% ethanol by vortexing thoroughly, and dried overnight at 60 °C, after which the weight was determined. The percentage weight reduction was determined using the formula ((Initial weight- Final weight)/Initial weight) × 100.

Further, the PP strips were also subjected to whole cell lysate treatment with repeated replenishment of the enzyme after every 3 days for a period of 15 days to achieve improved degradation. Chemical changes in the biodegraded plastic strip were observed by using NMR and FTIR.

The degradation activity of the enzyme was also confirmed by setting up a different set of control experiments wherein the PP strip was incubated for 3 days with only the buffer, with crude cell lysate of empty pET vector expressed in *E. coli* Shuffle strain, and using the whole cell lysate of the enzyme after heat inactivation. For heat inactivation, the enzyme was incubated at 100 °C for 1 h, and then the lysate was incubated with a PP strip at 60 °C for 3 days. Chemical and morphological changes in the plastic strip were observed by using SEM and FTIR.

The biodegradation rate constant of PP samples reduction was also determined by using the first-order kinetic model based on the initial and final weights along specific intervals[74]. The equation was as follows:

$$K = -\frac{1}{t}\left(ln\frac{W}{W_0}\right)$$

Where, K is the first-order rate constant for PP samples uptake per day, W is the weight of residual PP samples (mg) and W_0 is the initial weight of PP samples (mg), and t is time in days. This model was adopted as it gives a constant fraction per unit time present or removed within the PP samples. A plot of ln $[W/W_0]$ vs. time was also plotted, which yields a straight line giving a slope of K (day^{-1}), which is the biodegradation rate constant.

To rule out the possibility that the observed activity was not due to additives or impurities present in commercial plastic, and to confirm that the enzyme targets the polymer itself, polypropylene (PP) pellets with 99% purity (Sigma-Aldrich) were incubated with the crude lysate of the MCO at 60 °C for 3 days in duplicates. The samples were then analyzed to evaluate the extent of degradation.

Nuclear magnetic resonance (NMR)

^{1}H NMR of the suspension obtained from the biodegradation process was performed using Bruker Advance 800 Spectrometer. The control and sample were dissolved in 1 ml of chloroform-d at 70 °C and change in chemical shift was analyzed by acquiring the spectra with spectral width of 8.01 KHz, pulse angle of 90° (14 µs) and a delay time for 1 s.

Fourier-transform infrared spectroscopy (FTIR)

FTIR Spectroscopy of the biodegraded plastic strips was performed to determine the functional groups and the oxidative activity of the enzyme. FTIR Spectroscopy was done using FTIR ThermoFisher Scientific Nicolet iS50 in ATR mode, considering a range of 500–5000 cm^{-1}. To assess the changes on the PP strip, due to mere adsorption of the enzyme, FTIR analysis was performed on the PP strip treated with the inactive enzyme.

Scanning electron microscopy (SEM)

The surface modification of the biodegraded plastic of PP was analyzed by SEM to determine the extent of damage that might have occurred on the surface of plastic strip or on the edges due to the action of enzyme. The plastic strips were completely dried, and the samples were then carefully mounted onto the sample holder by using carbon tape. Samples were coated with gold prior to SEM analysis (ZEISS EVO Series Scanning Electron Microscope EVO 18).

Gas chromatography-mass spectrometry (GC-MS)

Presence of different compounds in control and biodegradation samples of PP strip (obtained from Sigma-Aldrich) was identified by GC-MS analysis using n-hexane as a solvent. Degradation products were extracted from the lysate solution using n-hexane in a 1:1 (v/v) ratio, followed by vortexing for 15 min. The mixture was then left undisturbed to allow phase separation. The organic (n-hexane) layer was carefully collected, air-dried to concentrate the sample, and subsequently reconstituted in 1 mL of n-hexane. The solution was filter-sterilized and transferred into HPLC vials for analysis. Five microlitres of the sample were injected into an Agilent J&W HP-5 precision-engineered (5%-phenyl)-methylpolysiloxane non-polar column of Agilent GC-MS 8860. The GC-MS operating conditions were as follows: helium (carrier gas) flow rate, 2 mL min^{-1}; oven program started at 50 °C (2 min hold), ramp rate 20 °C min^{-1} for 8 min, 300 °C final temperature; solvent delay, 6 min; split less injection; for detection and electron ionization at 70 eV. Identification of the degradation products was achieved by comparison of their mass spectra with the NST database, and checked by comparison of the retention times with the NST database.

Intact mass analysis

The purified MCO sample was loaded on the Agilent Advanced Bio 6545XT LC/QTOF (Agilent, USA) equipped with the PLRP-S, 1000A, and 1 mm column (Agilent, USA). Chromatographic parameters included mobile

phase A containing 100% water and mobile phase B 100% acetonitrile with the flow rate of 0.4 mL/min, injection volume of 5 µL, column compartment temperature of 60 °C. After chromatographic separation, the sample was subjected to MS analysis (Agilent 6545XT-QTOF).

Peptide mapping

Reversed-phase-HPLC (RP-HPLC) was performed using an Agilent 1260 Infinity Bio-inert Quaternary LC system linked to an Agilent 6230 ESI-TOF-MS apparatus operating in data-dependent mode on an Advance Bio peptide mapping C18 (4.6 × 150 mm, 2.7 mm, Agilent Technologies) column operated at 55 °C. The column was pre-saturated with 5% mobile phase B and 95% mobile phase A (0.1% v/v FA in acetonitrile and MilliQ water, respectively), prior to injection. Separation was performed from 5% to 65% B at a flow rate of 0.5 mL/min over a 35-min linear gradient. Monitoring UV absorbance at 214 nm and TIC data for *m/z* 100–3200 were used to achieve the detection. Prior to analysis, the MS spectra were calibrated in positive ion mode. The capillary gas temperature/Vcap and Vfrag were both adjusted to 300 °C and 4500 V, respectively. In silico Avastin peptide masses were matched with the masses of the likely peptides from the MS spectrum using the protein molecular feature extraction method in the Agilent MassHunter Qualitative Analysis and BioConfirm software with a tolerance of 10.0 ppm to determine sequence coverage.

Protein and ligand preparation

The complete amino acid sequence of the protein was aligned against a PDB database to predict the reference structure[75]. The 3D structure of the novel MCO extracted from *Micrococcus* sp. IITD107 was predicted using homology modeling with the reference structure[76,77]. Further, three copper atoms were placed at three sites identified by superimposing the crystal structure of Laccase B (PDB: 3KW7)[78]. The protein structure was then used for docking studies to understand the binding of polypropylene with MCO[79,80]. The enzymatic catalysis of plastic molecules undergoes degradation when the polymer size typically ranges below 50 carbon atoms. Therefore, three-dimensional structures of the monomer, 10-mer, and 30-mer of PP were generated using ChemSketch software[81]. These structures were then cleaned, optimized, and exported in PDBQT format.

Docking of multi-copper oxidase with different forms of plastic polymers

Protein-ligand docking of each form of PP on the predicted structure of MCO was performed using AutoDock[79,82]. The predicted protein structure was prepared for docking by adding polar hydrogens, Kollman charges to the protein molecules, and valency (+2) to the copper ions. Ligands were kept flexible during docking. The MCO used in this study is found to be novel to the best of our knowledge, and therefore, no active sites are known. Therefore, blind docking was initially performed for the 10-mer form of PP to explore the entire protein surface and predict the most probable active binding site. This site was then used for site-directed docking of the other PP variants (2-mer and 30-mer) to ensure consistency in the binding pocket across all forms. A genetic algorithm (GA) was used for docking, with a total of 50 GA runs, a population size of 500, and 2,500,000 evaluations to search for the best conformational space for all forms of PP[79]. The binding free energy of each PP variant with *Micrococcus* and *Rhodococcus* MCO was evaluated. Different types of interactions formed between the enzyme and the 10-mer polypropylene complex after docking were visualized using BIOVIA Discovery Studio 4.5[83,84].

Molecular dynamics simulation of the multi-copper oxidase and plastic polymer complexes

Molecular dynamics simulations were performed using the Desmond package of Schrodinger with the OPLS force field to evaluate the stability of MCO with a 10-mer polypropylene complex in an explicit solvent environment[85]. The MCO-PP complex was solvated in a TIP3P water model within a cubic periodic boundary box, maintaining a 10 Å buffer between the complex and the box edges to prevent self-interactions across periodic images[86]. Further, the system was neutralized by adding counterions. Energy minimization was conducted for 10 ns to relax the system and ensure structural stability before the production run. Minimization involved a two-step approach: an initial phase using the steepest descent algorithm to rapidly reduce large forces, followed by the conjugate gradient method for fine-tuning the energy landscape of the system[87,88]. The minimized systems underwent 120 ns of MD simulation under NPT ensemble conditions, maintaining a temperature of 338 K, a pressure of 1 atm, and an integration time step of 2 fs to assess the long-term stability and dynamic behavior of the complexes[89]. The trajectories generated after the simulation run were analyzed using the Desmond Simulation Event Analysis module. The root mean square deviation of the MCO-plastic polymer complex was estimated relative to the reference structure considered from the first frame over the 120-ns simulation. The stability of the polypropylene inside the active site of MCO was investigated as a function of time. The RMSF of residues in MCO was also analyzed to investigate the flexibility of protein regions interacting with the ligands. The MolSA, SASA, and rGyr were also calculated to assess the changes in protein conformation and solvent exposure throughout the simulation.

Data availability

The dataset used and analyzed during the current study is available from the corresponding author upon reasonable request.

Received: 5 September 2025; Accepted: 25 November 2025;
Published online: 30 December 2025

References

1. Lomwongsopon, P. & Varrone, C. Critical review on the progress of plastic bioupcycling technology as a potential solution for sustainable plastic waste management. *Polymers.* **14**, 4996 (2022).
2. Amobonye, A., Bhagwat, P., Singh, S. & Pillai, S. Plastic biodegradation: frontline microbes and their enzymes. *Sci. Total Environ.* **759**, 143536 (2021).
3. Lee, G. H. et al. Biotechnological plastic degradation and valorization using systems metabolic engineering. *Int. J. Mol. Sci.* **24**, 15181 (2023).
4. Tiso, T. et al. The metabolic potential of plastics as biotechnological carbon sources—review and targets for the future. *Metab. Eng.* **71**, 77–98 (2022).
5. Carlsen, L. & Bruggemann, R. The 17 United Nations' sustainable development goals: a status by 2020. *Int. J. Sustain. Dev. World Ecol.* **29**, 219–229 (2022).
6. Gilani, I. E., Sayadi, S., Zouari, N. & Al-Ghouti, M. A. Plastic waste impact and biotechnology: exploring polymer degradation, microbial role, and sustainable development implications. *Bioresour. Technol. Rep.* **24**, 101606 (2023).
7. Lee, S., Lee, Y. R., Kim, S. J., Lee, J.-S. & Min, K. Recent advances and challenges in the biotechnological upcycling of plastic wastes for constructing a circular bioeconomy. *Chem. Eng. J.* **454**, 140470 (2023).
8. Haider, T. P., Völker, C., Kramm, J., Landfester, K. & Wurm, F. R. Plastics of the future? The impact of biodegradable polymers on the environment and on society. *Angew. Chem. Int. Ed.* **58**, 50–62 (2019).
9. Pathak, V. M. Review on the current status of polymer degradation: a microbial approach. *Bioresour. Bioprocess.* **4**, 1–31 (2017).
10. Andler, R. et al. Current progress on the biodegradation of synthetic plastics: from fundamentals to biotechnological applications. *Rev. Environ. Sci. Bio/Technol.* **21**, 829–850 (2022).
11. Ali, S. S. et al. Plastic wastes biodegradation: mechanisms, challenges and future prospects. *Sci. Total Environ.* **780**, 146590 (2021).
12. Nugroho, R. A. A., Alhikami, A. F. & Wang, W.-C. Thermal decomposition of polypropylene plastics through vacuum pyrolysis. *Energy* **277**, 127707 (2023).

13. Grigoriadi, K. et al. The role of recycling in UV and thermal ageing of polypropylene block copolymer. *Polym. Degrad. Stab.* **222**, 110693 (2024).
14. Auta, H. S., Emenike, C. U., Jayanthi, B. & Fauziah, S. H. Growth kinetics and biodeterioration of polypropylene microplastics by Bacillus sp. and Rhodococcus sp. isolated from mangrove sediment. *Mar. Pollut. Bull.* **127**, 15–21 (2018).
15. Shimpi, N., Borane, M., Mishra, S., Kadam, M. & Sonawane, S. Biodegradation of isotactic polypropylene (iPP)/poly (lactic acid)(PLA) and iPP/PLA/nano calcium carbonates using phanerochaete chrysosporium. *Adv. Polym. Technol.* **37**, 522–530 (2018).
16. Skariyachan, S. et al. Enhanced polymer degradation of polyethylene and polypropylene by novel thermophilic consortia of Brevibacillus sps. and Aneurinibacillus sp. screened from waste management landfills and sewage treatment plants. *Polym. Degrad. Stab.* **149**, 52–68 (2018).
17. Wichatham, K. et al. Biodegradation of polypropylene plastics in vitro and natural condition by Streptomyces sp. isolated from plastic-contaminated sites. *Environ. Technol. Innov.* **35**, 103681 (2024).
18. Auta, S., Emenike, C. & Fauziah, S. Screening for polypropylene degradation potential of bacteria isolated from mangrove ecosystems in Peninsular Malaysia. *Int. J. Biosci. Biochem. Bioinform.* **7**, 245–251 (2017).
19. Tan, Q. et al. The programmed sequence-based oxygenase screening for polypropylene degradation. *J. Hazard. Mater.* **465**, 133173 (2024).
20. Arregui, L. et al. Laccases: structure, function, and potential application in water bioremediation. *Microb. Cell Factories* **18**, 1–33 (2019).
21. Morozova, O., Shumakovich, G., Shleev, S. & Yaropolov, Y. I. Laccase-mediator systems and their applications: a review. *Appl. Biochem. Microbiol.* **43**, 523–535 (2007).
22. Zargar, A. N. et al. Asphaltene biotransformation for heavy oil upgradation. *AMB Express* **11**, 1–19 (2021).
23. Zampolli, J. et al. Oxidative degradation of polyethylene by two novel laccase-like multicopper oxidases from Rhodococcus opacus R7. *Environ. Technol. Innov.* **32**, 103273 (2023).
24. Zampolli, J. et al. Transcriptomic analysis of Rhodococcus opacus R7 grown on polyethylene by RNA-seq. *Sci. Rep.* **11**, 21311 (2021).
25. Yoon, M. G., Jeon, H. J. & Kim, M. N. Biodegradation of polyethylene by a soil bacterium and AlkB cloned recombinant cell. *J. Bioremediation Biodegrad.* **3**, 1–8 (2012).
26. Restrepo-Flórez, J.-M., Bassi, A. & Thompson, M. R. Microbial degradation and deterioration of polyethylene—a review. *Int. Biodeterior. Biodegrad.* **88**, 83–90 (2014).
27. Kinkar, E., Kinkar, A. & Saleh, M. The multicopper oxidase of Mycobacterium tuberculosis (MmcO) exhibits ferroxidase activity and scavenges reactive oxygen species in activated THP-1 cells. *Int. J. Med. Microbiol.* **309**, 151324 (2019).
28. Brouwers, G.-J. et al. cumA, a gene encoding a multicopper oxidase, is involved in Mn2+ oxidation in Pseudomonas putida GB-1. *Appl. Environ. Microbiol.* **65**, 1762–1768 (1999).
29. Larsen, E. I., Sly, L. I. & McEwan, A. G. Manganese (II) adsorption and oxidation by whole cells and a membrane fraction of Pedomicrobium sp. ACM 3067. *Arch. Microbiol.* **171**, 257–264 (1999).
30. Palm-Espling, M. E., Niemiec, M. S. & Wittung-Stafshede, P. Role of metal in folding and stability of copper proteins in vitro. *Biochim. Biophys. Acta Mol. Cell Res.* **1823**, 1594–1603 (2012).
31. Harrison, M. D., Jones, C. E., Solioz, M. & Dameron, C. T. Intracellular copper routing: the role of copper chaperones. *Trends Biochem Sci.* **25**, 29–32 (2000).
32. Achila, D. et al. Structure of human Wilson protein domains 5 and 6 and their interplay with domain 4 and the copper chaperone HAH1 in copper uptake. *Proc. Natl. Acad. Sci. USA* **103**, 5729–5734 (2006).
33. Itoh, S. et al. Novel role of antioxidant-1 (Atox1) as a copper-dependent transcription factor involved in cell proliferation. *J. Biol. Chem.* **283**, 9157–9167 (2008).
34. Moro, G., Brissos, V., Zanardi, C., Martins, L. O. & Conzuelo, F. Electrochemical investigations of the multicopper oxidase from Aquifex aeolicus under direct electron transfer with carbon electrodes. *Electrochim. Acta.* **468**, 143199 (2023).
35. Chumillas, S. et al. Comprehensive study of the enzymatic catalysis of the electrochemical oxygen reduction reaction (ORR) by immobilized copper efflux oxidase (CueO) from Escherichia coli. *Front. Chem.* **6**, 358 (2018).
36. Mattos, G. J. et al. Electrochemical characterization of the laccase-catalyzed oxidation of 2,6-dimethoxyphenol: an insight into the direct electron transfer by enzyme and enzyme-mediator system. *Appl. Biochem. Biotechnol.* **194**, 4348–4361 (2022).
37. Zhou, G. et al. Determination of reactive oxygen species generated in laccase catalyzed oxidation of wood fibers from Chinese fir (Cunninghamia lanceolata) by electron spin resonance spectrometry. *Bioresour. Technol.* **100**, 505–508 (2009).
38. Cardullo, N., Muccilli, V. & Tringali, C. Laccase-mediated synthesis of bioactive natural products and their analogues. *RSC Chem. Biol.* **3**, 614–647 (2022).
39. Janusz, G. et al. Laccase Properties, Physiological Functions, and Evolution. *Int. J. Mol. Sci.* **21**, 966 (2020).
40. Baiocco, P., Barreca, A. M., Fabbrini, M., Galli, C. & Gentili, P. Promoting laccase activity towards non-phenolic substrates: a mechanistic investigation with some laccase–mediator systems. *Org. Biomol. Chem.* **1**, 191–197 (2003).
41. Galletti, P. et al. Laccase-mediator system for alcohol oxidation to carbonyls or carboxylic acids: toward a sustainable synthesis of profens. *ChemSusChem.* **7**, 2684–2689 (2014).
42. Harper, C. A. *Handbook of Plastics, Elastomers, and Composites* Vol. 4 (McGraw-Hill, 1996).
43. Steller, R. & Meissner, W. Structure and properties of degradable polyolefin-starch blends. *Polym. Degrad. Stab.* **60**, 471–480 (1998).
44. Cacciari, I. et al. Isotactic polypropylene biodegradation by a microbial community: physicochemical characterization of metabolites produced. *Appl. Environ. Microbiol.* **59**, 3695–3700 (1993).
45. Iwamoto, A. & Tokiwa, Y. Enzymatic degradation of plastics containing polycaprolactone. *Polym. Degrad. Stab.* **45**, 205–213 (1994).
46. Alariqi, S. A., Kumar, A. P., Rao, B. & Singh, R. Biodegradation of γ-sterilised biomedical polyolefins under composting and fungal culture environments. *Polym. Degrad. Stab.* **91**, 1105–1116 (2006).
47. Kaczmarek, H., Ołdak, D., Malanowski, P. & Chaberska, H. Effect of short wavelength UV-irradiation on ageing of polypropylene/cellulose compositions. *Polym. Degrad. Stab.* **88**, 189–198 (2005).
48. Huang, C.-Y., Roan, M.-L., Kuo, M.-C. & Lu, W.-L. Effect of compatibiliser on the biodegradation and mechanical properties of high-content starch/low-density polyethylene blends. *Polym. Degrad. Stab.* **90**, 95–105 (2005).
49. Ramis, X. et al. Thermal degradation of polypropylene/starch-based materials with enhanced biodegradability. *Polym. Degrad. Stab.* **86**, 483–491 (2004).
50. Arkatkar, A., Juwarkar, A. A., Bhaduri, S., Uppara, P. V. & Doble, M. Growth of Pseudomonas and Bacillus biofilms on pretreated polypropylene surface. *Int. Biodeterior. Biodegrad.* **64**, 530–536 (2010).
51. Morancho, J. et al. Calorimetric and thermogravimetric studies of UV-irradiated polypropylene/starch-based materials aged in soil. *Polym. Degrad. Stab.* **91**, 44–51 (2006).
52. Kathiresan, K. Polythene and plastics-degrading microbes from the mangrove soil. *Rev. Biol. Trop.* **51**, 629–633 (2003).

53. Montazer, Z., Habibi Najafi, M. B. & Levin, D. B. "Microbial degradation of low-density polyethylene and synthesis of polyhydroxyalkanoate polymers". *Can. J. Microbiol.* **65**, 224–234 (2019).
54. Shah, A. A., Hasan, F., Hameed, A. & Ahmed, S. Biological degradation of plastics: A comprehensive review. *Biotechnol. Adv.* **26**, 246–265 (2007).
55. Emmanuel-Akerele, H. A., Akinyemi, P. & Igbogbo-Ekpunobi, O. E. "Isolation and identification of plastic degrading bacteria from dumpsites Lagos".1 ():. *Adv. Environ. Technol.* **8**, 59–71 (2022).
56. Ghatge, S., Yang, Y, Ahn, J. H. & Hur, H. G. Biodegradation of polyethylene: a brief review. *Appl. Biol. Chem.* **63**, 27 (2020).
57. Zhang, A., Hou, Y., Wang, Q. & Wang, Y. Characteristics and polyethylene biodegradation function of a novel cold-adapted bacterial laccase from Antarctic sea ice psychrophile Psychrobacter sp. NJ228. *J. Hazard. Mater.* **439**, 129656 (2022).
58. Wasserbauer, R., Beranova, M., Vancurova, D. & Doležel, B. Biodegradation of polyethylene foils by bacterial and liver homogenates. *Biomaterials* **11**, 36–40 (1990).
59. Yang, J., Yang, Y., Wu, W.-M., Zhao, J. & Jiang, L. Evidence of polyethylene biodegradation by bacterial strains from the guts of plastic-eating waxworms. *Environ. Sci. Technol.* **48**, 13776–13784 (2014).
60. Yao, C., Xia, W., Dou, M., Du, Y. & Wu, J. Oxidative degradation of UV-irradiated polyethylene by laccase-mediator system. *J. Hazard. Mater.* **440**, 129709 (2022).
61. Zhang, X. et al. Degradation of polyethylene by Klebsiella pneumoniae Mk-1 isolated from soil. *Ecotoxicol. Environ. Saf.* **258**, 2023 (2023).
62. Telke, A. A., Ghodake, G. S., Kalyani, D. C., Dhanve, R. S. & Govindwar, S. P. Biochemical characteristics of a textile dye degrading extracellular laccase from a Bacillus sp. ADR. *Bioresour. Technol. Rep.* **102**, 1752–1756 (2011).
63. Wang, H. et al. Characterization and application of a novel laccase derived from Bacillus amyloliquefaciens. *Int. J. Biol. Macromol.* **150**, 982–990 (2020).
64. Neelkant, K. S., Shankar, K., Jayalakshmi, S. K. & Sreeramulu, K. Purification, biochemical characterization, and facile immobilization of laccase from Sphingobacterium ksn-11 and its application in transformation of diclofenac. *Appl. Biochem. Biotechnol.* **192**, 831–844 (2020).
65. Enyoh, C. E., Wang, Q., Ovuoraye, P. E. & Maduka, T. O. Toxicity evaluation of microplastics to aquatic organisms through molecular simulations and fractional factorial designs. *Chemosphere* **308**, 136342 (2022).
66. Ray, A. S., Rajasekaran, M., Uddin, M. & Kandasamy, R. Laccase driven biocatalytic oxidation to reduce polymeric surface hydrophobicity: An effective pre-treatment strategy to enhance biofilm mediated degradation of polyethylene and polycarbonate plastics. *Sci. Total Environ.* **904**, 166721 (2023).
67. Satomura, T. akenori et al. Activity enhancement of multicopper oxidase from a hyperthermophile via directed evolution, and its application as the element of a high performance biocathode. *J. Biotechnol.* **325**, 226–232 (2021).
68. Takamura, E. et al. Site-directed mutagenesis of multicopper oxidase from hyperthermophilic archaea for high-voltage biofuel cells. *Appl. Biochem. Biotechnol.* **193**, 492–501 (2020).
69. Ma, Y., Tayefi, S. H., Mogharabi-Manzari, M. & Luo, X. Advances in immobilized enzyme systems for enhanced microplastic biodegradation: a review. *Int. J. Biol. Macromol.* **328**, 147656 (2025).
70. Wojnowska-Baryła, I., Bernat, K. & Zaborowska, M. Plastic waste degradation in landfill conditions: the problem with microplastics, and their direct and indirect environmental effects. *Int. J. Environ. Res. Public Health* **19**, 13223 (2022).
71. Singh, P., Chachan, S., Singhi, D. & Srivastava, P. Isolation and molecular characterization of a stationary phase promoter useful for gene expression in Gordonia. *Gene* **591**, 153–160 (2016).
72. Jhadav, A. et al. Optimization of production and partial purification of laccase by Phanerochaete chrysosporium using submerged fermenation. *Int. J. Microbiol. Res.* **1**, 9 (2009).
73. Lonhienne, T., Gerday, C. & Feller, G. Psychrophilic enzymes: revisiting the thermodynamic parameters of activation may explain local flexibility. *Biochim. Biophys. Acta Protein Struct. Mol. Enzymol.* **1543**, 1–10 (2000).
74. Samat, A. F., Carter, D. & Abbas, A. Biodeterioration of pre-treated polypropylene by Aspergillus terreus and Engyodontium album. *npj Mater. Degrad.* **7**, 28 (2023).
75. Rose, P. W. et al. The RCSB Protein Data Bank: new resources for research and education. *Nucleic Acids Res.* **41**, D475–D482 (2012).
76. Kiefer, F., Arnold, K., Künzli, M., Bordoli, L. & Schwede, T. The SWISS-MODEL Repository and associated resources. *Nucleic Acids Res.* **37**, D387–D392 (2009).
77. Schwede, T., Kopp, J., Guex, N. & Peitsch, M. C. SWISS-MODEL: an automated protein homology-modeling server. *Nucleic Acids Res.* **31**, 3381–3385 (2003).
78. Ge, H. et al. Structure of native laccase B from Trametes sp. AH28-2. *Struct. Biol. Cryst. Commun.* **66**, 254–258 (2010).
79. Morris, G. M. et al. Automated docking using a Lamarckian genetic algorithm and an empirical binding free energy function. *J. Comput. Chem.* **19**, 1639–1662 (1998).
80. Brooijmans, N. & Kuntz, I. D. Molecular recognition and docking algorithms. *Annu. Rev. Biophys. Biomol. Struct.* **32**, 335–373 (2003).
81. ACD, V. & Elucidator, S. Advanced Chemistry Development, Inc., (Toronto, ON, Canada, 2019).
82. Morris, G. M. et al. AutoDock4 and AutoDockTools4: automated docking with selective receptor flexibility. *J. Comput. Chem.* **30**, 2785–2791 (2009).
83. Accelrys Software Inc. Discovery Studio Modeling Environment, Release 2.0, (San Diego: Accelrys Software Inc., 2008).
84. Visualizer, D. Discovery Studio visualizer. 2. (Accelrys Software Inc., Waltham, United States, 2005).
85. Bowers, Kevin J. et al. "Scalable algorithms for molecular dynamics simulations on commodity clusters." In *Proceedings of the 2006 ACM/IEEE Conference on Supercomputing*. (2006).
86. Jorgensen, W. L., Chandrasekhar, J., Madura, J. D., Impey, R. W. & Klein, M. L. Comparison of simple potential functions for simulating liquid water. *J. Chem. Phys.* **79**, 926–935 (1983).
87. Hoover, W. G. Canonical dynamics: Equilibrium phase-space distributions. *Phys. Rev. A.* **31**, 1695 (1985).
88. Martyna, G. J., Tobias, D. J. & Klein, M. L. Constant pressure molecular dynamics algorithms. *J. Chem. Phys.* **101**, 10.1063 (1994).
89. Essmann, U. et al. A smooth particle mesh Ewald method. *J. Chem. Phys.* **103**, 8577–8593 (1995).

Acknowledgements

The authors would like to thank Prof. Lucinda E. Doyle for her help in determining the redox potential of the enzyme. The authors would like to thank ITC Limited for financial support and the Indian Institute of Technology Delhi for providing the infrastructure to conduct this research.

Author contributions

P.KU., R.K., A.N.Z., S.H., P.K: methodology, software, data curation, investigation, writing—original draft preparation. M.C., B.B., D.C.: visualization. P.S.: conceptualization. D.S., A.S.R., P.S.: supervision. M.C., B.B., D.C., D.S., A.S.R., P.S.: writing—reviewing and editing.

Competing interests
All the authors declare no financial or non-financial competing interests.

Additional information
Supplementary information The online version contains supplementary material available at https://doi.org/10.1038/s41529-025-00720-5.

Correspondence and requests for materials should be addressed to Preeti Srivastava.